International Journal of Solids and Structures 269 (2023) 112167

Contents lists available at ScienceDirect

International Journal of Solids and Structures

journal homepage: www.elsevier.com/locate/ijsolstr

Thermoelastic fields for a heat exchanger of arbitrary shape in a bi-material infinite plane

Chunlin Wu [a,b], Huiming Yin [b,*]

[a] Shanghai Institute of Applied Mathematics and Mechanics, Shanghai Key Laboratory of Mechanics in Energy Engineering, Shanghai Frontier Science Center of Mechanoinformatics, School of Mechanics and Engineering Science, Shanghai University, Shanghai 200072, China
[b] Department of Civil Engineering and Engineering Mechanics, Columbia University, 610 Seeley W. Mudd 500 West 120th Street, NY, 10027, United States of America

ARTICLE INFO

Keywords:
Bi-material Green's functions
Polygonal particles
Polynomial eigenstrain
Eshelby's tensor
Equivalent inclusion method
Thermoelastic analysis

ABSTRACT

When a bi-material with two jointed dissimilar half-planes containing an arbitrarily shaped polygonal inclusion is subjected to heat flow, the thermoelastic fields, including temperature and displacement, can be derived by the Green's function technique with the integral of the source over the inclusion. Using Hadamard's regularization, the two-dimensional (2D) thermal, elastic, and thermoelastic Green's functions of two-jointed dissimilar half-planes are firstly derived from the 3D Green's functions as the corresponding fundamental solutions. The fundamental solutions for semi-infinite and infinite domains can be recovered by adjusting the material constants. Eshelby's tensors are derived in terms of the biharmonic, harmonic, and two Boussinesq's displacement potential functions. When a heat exchanger of arbitrary shape is embedded in a matrix with different thermal and mechanical properties, combining a continuously distributed eigen-temperature gradient and eigenstrain field, the dual equivalent inclusion method (DEIM) is applied to handle the material mismatch of thermal conductivity, stiffness, and thermal expansion coefficient, respectively. Therefore, the full thermoelastic fields can be obtained by the integral over the heat exchanger only. The eigen-fields are expanded in the Taylor series referred to the center of the particle, which exhibits tailorable accuracy with uniform, linear or quadratic terms in comparison with the analytical solution for a circular inhomogeneity in the infinite domain. An exact thermoelastic solution of a circular inhomogeneity embedded within the infinite domain is present. The case study of an electric heat cable in the concrete block demonstrates the capability and exactness of the model. The method can be used for a thin film containing a heat exchanger of arbitrary shape as either a heat sink or source.

1. Introduction

In Eshelby's celebrated works of the equivalent inclusion method (EIM) (Eshelby, 1957, 1959), the ellipsoidal inhomogeneity is replaced by inclusion with uniformly distributed eigenstrain but the same stiffness as the matrix. Hence, the original boundary value problem was mathematically transformed into the determination of eigenstrain with the equivalent stress conditions, which elegantly avoids the interface continuity with the multiple material domains. Due to its simplicity, the EIM has been widely applied in several micromechanical models (Zaoui, 2002). Particularly, the investigation of effective material properties attracts extensive interest, such as (Mori and Tanaka, 1973), self-consistent (Kroner, 1958; Hershey, 1954) methods, which aim to illustrate the relationship between microstructures and macroscopic behaviors. Thanks to the versatility of Green's functions to various problems, other physical inhomogeneity problems have been explored with EIM, such as transient heat conduction (Wu et al., 2021a), magneto-elasticity (Yin et al., 2006), and subsequent extensions on double- or multi-layered inclusion methods (Hori and Nemat-Nasser, 1993).

Among the micromechanical models, strong assumptions are generally made on spatial averaged strain/stress fields and ellipsoidal shapes of inhomogeneity. When a particle's shape is arbitrary, the local fields may not be accurately obtained as Eshelby's tensor in the particle domain exhibits significant variation and is singular in the neighborhood of vertices. Note that the domain integrals of second-order derivatives of Green's function for an infinite domain of a single material over an ellipsoidal inclusion, namely the Eshelby's tensor, is uniform at the field point within the inclusion, which provides the exact and elegant solution for a single ellipsoidal/elliptic particle in an infinite domain under a uniform far field. For a polygonal inhomogeneity, Eshelby's is not constant over the particle anymore, and eigenstrain

* Corresponding author.
E-mail addresses: cw3056@columbia.edu (C. Wu), yin@civil.columbia.edu (H. Yin).

https://doi.org/10.1016/j.ijsolstr.2023.112167
Received 8 December 2022; Received in revised form 5 February 2023; Accepted 14 February 2023
Available online 24 February 2023

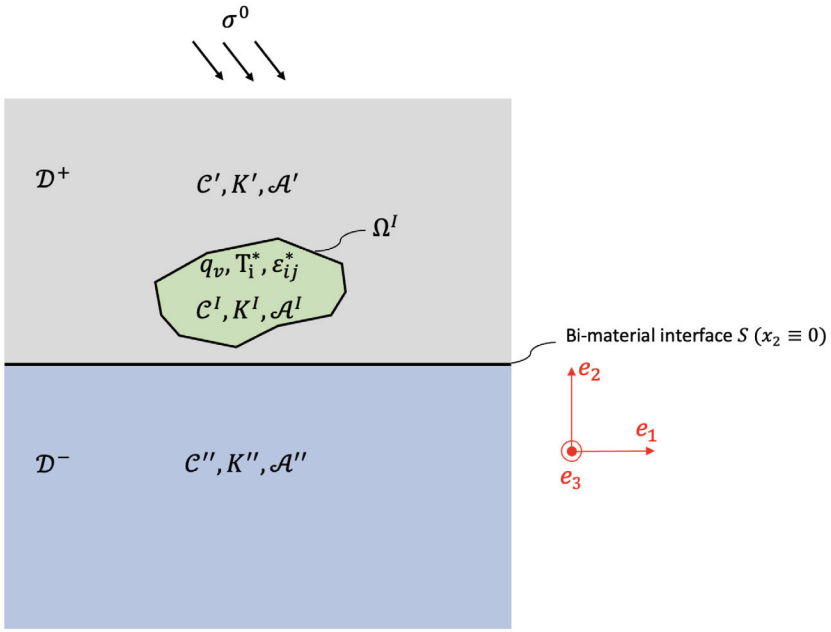

Fig. 1. Schematic illustration of a cross-section D composed of two jointed dissimilar half spaces D^+, D^- subjected to far-field load σ^0, embedded with an arbitrarily-shaped polygonal inhomogeneity Ω^I, where exist heat source q_v and eigen-fields T_i^* and ε_{ij}^*.

varies on the particle as well. In addition, eigen-fields can be disturbed by (i) interactions of multiple inhomogeneities (Moschovidis and Mura, 1975); and (ii) boundary effects (Wu and Yin, 2021b), including the bi-material interfacial perturbation (Wu et al., 2023b).

To approximate variations of eigen-fields, polynomials are first introduced by Moschovidis and Mura (Moschovidis and Mura, 1975), where the eigen-fields are expanded at the center of inhomogeneity with the Taylor series. Subsequently, Brisard et al. (2014) proposed a variational EIM for numerical homogenization. On the other hand, unlike elliptical subdomains, Gao and Ma (2010) and Trotta et al. (2017) have shown that Eshelby's tensor varies within polygons. Even for an elliptical/ellipsoidal subdomain embedded in bi-material space, the internal Eshelby's tensor is not uniform anymore due to the term of $\Theta^u = \int_\Omega \alpha^u d\mathbf{x}'$ in Wu et al. (2023b) produced by the image source. The Eshelby's tensor for polygons in bi-material has not been solved in the literature yet.

Since the two above conditions can seldom be satisfied, to provide more accurate solutions, this paper follows the previous work in a single material domain (Rodin, 1996; Wu and Yin, 2021a) to derive Eshelby's tensors of polygonal subdomains with polynomial eigenstrain, but the bi-material thermoelastic Green's functions will be used. In the literature, pioneers have investigated inclusion problems and related Eshelby's tensors for specific polygonal subdomains. For cuboids, Chiu (1977, 1978, 1980) provided closed-form stress fields caused by uniform initial strain for full- and half-space; Ru (1999) obtained internal stresses of an arbitrarily shaped inclusion through explicit expressions. Based on Waldvogel (1979) work on the Newtonian potential of a homogeneous polyhedron, Rodin (1996) firstly proposed Eshelby's tensors for arbitrarily shaped polygonal and polyhedral inclusions through Gauss' theorem. Subsequently, Gao and Ma (2010) provided Eshelby's tensor combined with strain gradient theory; Trotta et al. (2017) applied Green's theorem and expressed Eshelby's tensors merely through coordinates of vertices on inclusions; Nozaki and Taya (1997, 2000) proposed closed-form Eshelby's tensors for arbitrary polygons, which are only applicable to convex cases. The above works can provide exact solutions for inclusion problems with uniform eigenstrain, which exhibit the same material properties as the matrix. Besides, the critical application of Eshelby's tensors is a solution to inhomogeneity problems, which requires considering variations of eigen-fields. Therefore, Wu and Yin (2021a) directly integrated Eshelby's tensor without Green's theorem and extended it to polynomial-form eigenstrains for EIM.

Research on fundamental solutions has a long tradition, and particularly extensive efforts have been devoted to elastic and thermoelastic fields. Walpole (1996) obtained a simple and explicit solution when the source point is located in the upper layer, which was later completed by Wu et al. (2022). As for research on thermoelasticity, Nowacki (1986) first proposed a three-dimensional full-space thermoelastic fundamental solution, later summarized by Barber (1992) with two-dimensional cases. Following Yu and Sanday (1991) on an inclusion problem with nuclei strain and Goodier's method, Yu et al. (1992) proposed a bi-material thermoelastic solution caused by eigenstrain (thermal strain) within a spherical inclusion. Subsequently, Hou's group (Hou et al., 2013b,a) applied four harmonic potential functions to represent general and fundamental solutions in cylindrical coordinates, significantly simplifying trivial expressions. Following their general solutions, Wu et al. (2023a) proposed a thermoelastic bi-material fundamental solution in Cartesian coordinates and modified it for Eshelby's problem.

This paper aims to derive 2D Eshelby's tensors for polynomial eigen-fields in thermal, elastic, and thermoelastic problems under the plane strain condition. The plane stress problem can be easily obtained by changing the elastic constants with the same mathematical formulation (Mura, 1987). The representation of eigen-fields through polynomial distribution could provide tailorable accuracy with uniform, linear and quadratic terms, although it is not the exact solution as the elliptical/ellipsoidal inhomogeneity embedded in an infinite medium. Using the DEIM (Wu et al., 2023a), the induced thermal effects on elastic fields are fully coupled and handled through thermoelastic Eshelby's tensor on the polygonal subdomain, which avoids entire domain integrals of temperature. The DEIM can also be extended to three-dimensional problems with arbitrary polyhedral inhomogeneities. The domain integrals of the potential functions can be evaluated over the transformed coordinates (Rodin, 1996; Kuvshinov, 2008). Wu et al. (2021b) extended the method to polynomial eigen-fields, but the domain integrals of the Boussinesq's displacement potentials on the polyhedral inclusion were still open and may be provided in the future work. Section 2 presents 2D thermal, elastic, and thermoelastic bi-material fundamental solutions, which are straightforwardly derived using Hadamard's regularization. Section 3 provides

domain integrals of several Boussinesq's displacement potentials and extends to higher-order polynomial forms, precisely the linear and quadratic terms. Subsequently, domain integrals over a circular subdomain are elaborated for readers' interest in the applications of pipes. In Section 4, numerical verification is conducted to evaluate Eshelby's tensor of a circular inclusion with prescribed thermal strain. Section 5 conducted a case study of a single electric heat cable embedded in a concrete block for heat flux and thermal stress analyses.

2. Formulation

Consider an infinite domain D composed of two isotropic jointed dissimilar half spaces, where the upper and lower phases are D^+ and D^-, respectively. Without the loss of any generality, the bi-material interface S is assumed as plane x_1-x_3 with $x_2 \equiv 0$. When the bi-material medium D is embedded with an isotropic infinite long cylindrical inhomogeneity Ω^I parallel to x_3 axis, the three-dimensional model can be reduced to plane strain problem in x_1, x_2 axes. In general, shown as Fig. 1, two phases and inhomogeneity exhibit different material properties, specifically, (i) thermal conductivity K', K'', K^I; (ii) thermal modulus $\mathcal{A}', \mathcal{A}'', \mathcal{A}^I$; and (iii) elastic stiffness C', C'', C^I for D, D'' and Ω^I, respectively. For isotropic materials, the stiffness tensor $C_{ijkl} = \lambda\delta_{ij}\delta_{kl} + \mu(\delta_{ik}\delta_{jl} + \delta_{il}\delta_{jk})$, where λ and μ are two Lamé constants.

2.1. Two-dimensional fundamental solutions

The fundamental solutions relate excitation at source point $\mathbf{x}'$ and response at field point $\mathbf{x}$. Following conventional notations, let G denote the Green's function. Therefore the thermal (Wang et al., 2022), thermoelastic (Wu et al., 2023a) and elastic bi-material Green's function (Walpole, 1996; Wu et al., 2022) are expressed as G, G_i and G_{ij}, respectively, which are provided below. Although Eqs. (1)–(3) are originally applied for three-dimensional problems, they can be transformed into two-dimensional forms through Hadamard's regularization since they are composed of potential functions. Without the loss of any generality, this paper focus on the plane strain problem, and fundamental solutions for plane stress can be acquired by adjusting material constants.

Thermal bi-material fundamental solution

$$G(\mathbf{x},\mathbf{x}') = \begin{cases} \frac{1}{4\pi K^w}(\phi + \frac{K^w-K^s}{K^w+K^s}\overline{\phi}) & x_2'x_2 \geq 0 \\ \frac{1}{2\pi(K^w+K^s)}\phi & x_2'x_2 < 0 \end{cases} \tag{1}$$

Thermoelastic bi-material fundamental solution

$$G_i(\mathbf{x},\mathbf{x}') = \frac{1}{2\mu^w}\begin{cases} \mathcal{H}_5^w\psi_{,i} + (\mathcal{H}_1^w + L_B^y)\overline{\beta}_{,i}^y + L_B^y\overline{\psi}_{,i} \\ + x_2\Big[\chi\big(L_D^y - L_F^y\big)\overline{\alpha}_{,i}^y + L_C^y(\overline{\psi}_{,i2} + 2(1-2\nu^w)\delta_{i2}\overline{\phi} - x_2\overline{\phi}_{,i})\Big] & x_2x_2' \geq 0 \\ + \delta_{i2}\big[-(3-4\nu^w)\big(\mathcal{H}_3^w\overline{\alpha}^y + L_C^y\overline{\psi}_{,2}\big) + \chi\big(4(1-\nu^w)\mathcal{H}_6^w - L_B^y\big)\overline{\alpha}^y\big] \\ (\mathcal{H}_2^w + L_G^y)\beta_{,i}^y - x_2\Big[\mathcal{H}_4^w - L_G^y\Big]\alpha_{,i}^y + L_G^y\psi_{,i} \\ - \chi\delta_{i2}\alpha^I\Big[L_G^y + (3-4\nu^w)\mathcal{H}_4^w - 4(1-\nu^w)\mathcal{H}_7^w\Big] & x_2x_2' < 0 \end{cases} \tag{2}$$

Elastic bi-material fundamental solution

$$G_{ij}(\mathbf{x},\mathbf{x}') = \frac{1}{4\pi\mu^w}\begin{cases} (\delta_{ij}\phi - \frac{\psi_{,ij}}{4(1-\nu^w)}) + A^y\overline{\phi}\delta_{ij} + \chi B^y(\delta_{i2}\delta_{jk} - \delta_{ik}\delta_{j2})\overline{\alpha}_{,k}^y \\ - C^yx_2\Big[Q_J\overline{\psi}_{,ij2} + 4(1-\nu^w)\delta_{j2}\overline{\phi}_{,i} + 2(1-2\nu^w)\delta_{i2}Q_J\overline{\phi}_{,j} - Q_Jx_2\overline{\phi}_{,ij}\Big] & x_2'x_2 \geq 0 \\ - D^yQ_IQ_J\overline{\psi}_{,ji} - (G^y + B^y)Q_J\overline{\beta}_{,ij}^y \\ (\delta_{ij}\phi - \frac{\psi_{,ij}}{4(1-\nu^w)}) + A^y\phi\delta_{ij} + \chi B^y(\delta_{i2}\delta_{jk} - \delta_{ik}\delta_{j2})\alpha_{,k}^y \\ - D^y\psi_{,ij} - \chi x_2F^y\alpha_{,ij}^y - (G^y + B^y)Q_I\beta_{,ji}^y & x_2'x_2 < 0 \end{cases} \tag{3}$$

where (i) when $x_2' \geq 0$, $w = ', s = '', y = u$ and $\chi = 1$; and (ii) when $x_2' < 0$, $w = '', s = ', y = l$ and $\chi = -1$; $\overline{(.)}$ represents image terms, which is elaborated in Section 2.2 along with potential functions $\psi, \phi, \alpha, \beta$; matrix $\mathbf{Q} = (1, -1)$ handles negative partial derivatives with respect to x_2 direction. Following Mura's notation, the dummy index rule does not apply to capital characters. The material coefficients $\mathcal{H}_1^u, \mathcal{H}_2^u, \ldots, \mathcal{H}_7^u$, and $L_B^u, L_C^u, L_D^u, L_F^u$, and $A^u, B^u, C^u, D^u, F^u, G^u$ are provided as Eqs. (4)–(6), respectively.

$$\begin{aligned} \mathcal{H}_1^u &= \mathcal{H}_5^u - 2\mu'\Big[\frac{\mathcal{H}_7^u(1-\nu'')}{(3-4\nu'')\mu' + \mu''} + \frac{(\mathcal{H}_5^u + \mathcal{H}_6^u)(1-\nu')}{(3-4\nu')\mu'' + \mu'}\Big] \\ \mathcal{H}_2^u &= -2\mu''\Big[\frac{\mathcal{H}_7^u(1-\nu'')}{(3-4\nu'')\mu' + \mu''} + \frac{(\mathcal{H}_5^u + \mathcal{H}_6^u)(1-\nu')}{(3-4\nu')\mu'' + \mu'}\Big] \\ \mathcal{H}_3^u &= \frac{4\mathcal{H}_6^u(1-\nu')\mu'' - \mathcal{H}_5^u(\mu'-\mu'')}{(3-4\nu')\mu'' + \mu'}, \quad \mathcal{H}_4 = 4\mathcal{H}_7^u\frac{(1-\nu'')\mu'}{(3-4\nu'')\mu' + \mu''} \\ \mathcal{H}_5^u &= \frac{1}{8\pi K'}\frac{(1-2\nu')\mathcal{A}'}{1-\nu'}, \quad \mathcal{H}_6^u = \frac{1}{8\pi K'}\frac{(1-2\nu')\mathcal{A}'}{1-\nu'}\frac{K'-K''}{K'+K''}, \\ \mathcal{H}_7^u &= \frac{1}{4\pi(K'+K'')}\frac{(1-2\nu'')\mathcal{A}''}{1-\nu''} \end{aligned} \tag{4}$$

$$\begin{aligned} L_B^u &= \mathcal{H}_5^u\frac{(3-4\nu')(\mu'-\mu'')}{(3-4\nu')\mu'' + \mu'}, \quad L_C^u = 2\mathcal{H}_5^u\frac{(\mu'-\mu'')}{(3-4\nu')\mu'' + \mu'} \\ L_D^u &= \frac{4\mathcal{H}_6^u(1-\nu')\mu''}{(3-4\nu')\mu'' + \mu'}, \quad L_F^u = \frac{4\mathcal{H}_5^u(\mu'-\mu'')(1-\nu')}{(3-4\nu')\mu'' + \mu'} \end{aligned} \tag{5}$$

$$\begin{aligned} A^u &= \frac{\mu'-\mu''}{\mu'+\mu''}, \quad B^u = \frac{2\mu'(1-2\nu')(\mu'-\mu'')}{(\mu'+\mu'')(\mu'+\mu''(3-4\nu'))} \\ C^u &= \frac{\mu'-\mu''}{2(1-\nu')(\mu'+(3-4\nu')\mu'')}, \quad D^u = \frac{3-4\nu'}{2}C^u \\ F^u &= \frac{2\mu'(\mu'(1-2\nu'') - \mu''(1-2\nu'))}{(\mu'+\mu''(3-4\nu'))(\mu''+\mu'(3-4\nu''))} \\ G^u &= \frac{\mu'(\mu''(1-2\nu'')(3-4\nu') - \mu'(1-2\nu')(3-4\nu''))}{(\mu'+\mu''(3-4\nu'))(\mu''+\mu'(3-4\nu''))} \end{aligned} \tag{6}$$

2.2. Two-dimensional potential functions

Using Hadamard's regularization, the potential functions are integrated along x_3, and only finite parts are retained. The finite parts of two-dimensional bi-harmonic and harmonic potentials are shown in Eq. (7),

$$\begin{aligned} \psi &= -|\mathbf{x}-\mathbf{x}'|^2\frac{\ln|\mathbf{x}-\mathbf{x}'|^2 - 1}{2}, \quad \phi = -\ln|\mathbf{x}-\mathbf{x}'|^2 \\ \overline{\psi} &= -|\mathbf{x}-\overline{\mathbf{x}}'|^2\frac{\ln|\mathbf{x}-\overline{\mathbf{x}}'|^2 - 1}{2}, \quad \overline{\phi} = -\ln|\mathbf{x}-\overline{\mathbf{x}}'|^2 \end{aligned} \tag{7}$$

where $\overline{\mathbf{x}'} = (x_1', -x_2')$ or $\overline{x}_i' = Q_Ix_i'$. Although there exist infinite constants in ψ and $\overline{\psi}$, they vanish during partial differentiation to obtain Eshelby's tensors. For three-dimensional problems, four branches of α and β are shown as Eq. (5) in Wu et al. (2022), where the difference lies in integral limits. Following the same fashion, four branches of two-dimensional displacement potentials α are defined as Eq. (8),

$$\begin{aligned} \alpha^u(x_1,x_2) &= \int_{x_2}^{-\infty} -\ln[(x_1'-x_1)^2 + (x_2'-t)^2]\,dt \\ &= 2(x_1'-x_1)\arctan[\frac{x_1'-x_1}{x_2'-x_2}] + (x_2'-x_2)(\phi+2) \\ \overline{\alpha}^u(x_1,x_2) &= \int_{\infty}^{x_2} -\ln[(x_1'-x_1)^2 + (x_2'+t)^2]\,dt \\ &= 2(x_1'-x_1)\arctan[\frac{x_1'-x_1}{x_2'+x_2}] + (x_2'+x_2)(\overline{\phi}+2) \\ \alpha^l(x_1,x_2) &= \int_{\infty}^{x_2} -\ln[(x_1'-x_1)^2 + (x_2'-t)^2]\,dt \\ &= -2(x_1'-x_1)\arctan[\frac{x_1'-x_1}{x_2'-x_2}] - (x_2'-x_2)(\phi+2) \\ \overline{\alpha}^l(x_1,x_2) &= \int_{x_2}^{-\infty} -\ln[(x_1'-x_1)^2 + (x_2'+t)^2]\,dt \\ &= -2(x_1'-x_1)\arctan[\frac{x_1'-x_1}{x_2'+x_2}] - (x_2'+x_2)(\overline{\phi}+2) \end{aligned} \tag{8}$$

where $f(.)dx$ denote finite part integrals with respect to variable x; only finite parts are retained following two rules, (i) $\alpha^{u\&l}(\mathbf{x},\mathbf{x}')_{,i} = -\alpha^{u\&l}(\mathbf{x},\mathbf{x}')_{,i'}$, $\overline{\alpha}^{u\&l}(\mathbf{x},\mathbf{x}')_{,i} = -Q_I\overline{\alpha}^{u\&l}(\mathbf{x},\mathbf{x}')_{,i'}$; and (ii) partial derivatives of the finite part are equivalent to that of original expressions. Following the same fashion, the subsequent higher order displacement potential β can be determined as Eq. (9). Although relationships between finite parts are observed as $\beta^u = \beta^l$, $\overline{\beta}^u = \overline{\beta}^l$, the dropped constants in four branches of β are not exactly the same. Hence, one cannot simply conclude two potentials are equivalent unless in the sense of a finite part.

$$
\begin{aligned}
\beta^u(x_1,x_2) &= \fint_{x_2}^{-\infty}\alpha^u(x_1,t)dt \\
&= \frac{1}{2}\Big\{4(x_1'-x_1)(x_2'-x_2)\arctan[\frac{x_1'-x_1}{x_2'-x_2}] \\
&\quad + \big((x_2'-x_2)^2-(x_1'-x_1)^2\big)(\phi+3)\Big\} \\
\overline{\beta}^u(x_1,x_2) &= \fint_{\infty}^{x_2}\overline{\alpha}^u(x_1,t)dt \\
&= \frac{1}{2}\Big\{4(x_1'-x_1)(x_2'+x_2)\arctan[\frac{x_1'-x_1}{x_2'+x_2}] \\
&\quad + \big((x_2'+x_2)^2-(x_1'-x_1)^2\big)(\overline{\phi}+3)\Big\} \\
\beta^l(x_1,x_2) &= \fint_{\infty}^{x_2}\alpha^l(x_1,t)dt \\
&= \frac{1}{2}\Big\{4(x_1'-x_1)(x_2'-x_2)\arctan[\frac{x_1'-x_1}{x_2'-x_2}] \\
&\quad + \big((x_2'-x_2)^2-(x_1'-x_1)^2\big)(\phi+3)\Big\} \\
\overline{\beta}^l(x_1,x_2) &= \fint_{x_2}^{-\infty}\overline{\alpha}^l(x_1,t)dt \\
&= \frac{1}{2}\Big\{4(x_1'-x_1)(x_2'+x_2)\arctan[\frac{x_1'-x_1}{x_2'+x_2}] \\
&\quad + \big((x_2'+x_2)^2-(x_1'-x_1)^2\big)(\overline{\phi}+3)\Big\}
\end{aligned}
\tag{9}
$$

3. Domain integrals of two-dimensional Boussinesq's potentials

As illustrated in Section 1, due to boundary effects and interactions between inhomogeneities, the eigen-fields are approximated through the Taylor series as Eq. (10),

$$
\begin{aligned}
T_i^*(\mathbf{x}') &= T_i^{0*} + (x_k'-x_k^{Ic})T_{ik}^{1*} + (x_k'-x_k^c)(x_l'-x_l^c)T_{ikl}^{2*} + \cdots \\
\varepsilon_{ij}^*(\mathbf{x}') &= \varepsilon_{ij}^{0*} + (x_p'-x_p^c)\varepsilon_{ijp}^{1*} + (x_p'-x_p^c)(x_q'-x_q^c)\varepsilon_{ijpq}^{2*} + \cdots
\end{aligned}
\tag{10}
$$

where superscripts 0,1 and 2 represent the uniform, linear and quadratic terms, respectively; the superscript c stands for center of Ω^I; T_i^* and ε_{ij}^* are eigen-temperature gradient (ETG) and eigenstrain, respectively. Using the technique of Green's function, the induced thermal and elastic fields can be obtained,

$$
\begin{aligned}
T(\mathbf{x}) &= \int_\Omega G_{,i'}(\mathbf{x},\mathbf{x}')T_i^*(\mathbf{x}')\,d\mathbf{x}' \\
&= \int_\Omega G_{,i'}d\mathbf{x}'T_i^{0*} + \int_\Omega G_{,i'}(x_p'-x_p^c)d\mathbf{x}'T_{ip}^{1*} \\
&\quad + \int_\Omega G_{,i'}(x_p'-x_p^c)(x_q'-x_q^c)d\mathbf{x}'T_{ipq}^{2*} \\
&= D_iT_i^{0*} + D_{ip}T_{ip}^{1*} + D_{ipq}T_{ipq}^{2*} \\
u_i(\mathbf{x}) &= \int_\Omega G_{i,j'}(\mathbf{x},\mathbf{x}')T_j^*(\mathbf{x}') + G_{ij,k'}\varepsilon_{jk}^*(\mathbf{x}')\,d\mathbf{x}' \\
&= \int_\Omega G_{i,j'}d\mathbf{x}'T_j^{0*} + \int_\Omega G_{i,j'}(x_p'-x_p^c)d\mathbf{x}'T_{jp}^{1*} \\
&\quad + \int_\Omega G_{i,j'}(x_p'-x_p^c)(x_q'-x_q^c)d\mathbf{x}'T_{jpq}^{2*} \\
&\quad + \int_\Omega G_{ij,k'}d\mathbf{x}'\varepsilon_{jk}^{0*} + \int_\Omega G_{ij,k'}(x_p'-x_p^c)d\mathbf{x}'\varepsilon_{jkp}^{1*} \\
&\quad + \int_\Omega G_{ij,k'}(x_p'-x_p^c)(x_q'-x_q^c)d\mathbf{x}'\varepsilon_{jkpq}^{2*} \\
&= R_{ij}T_j^{0*} + R_{ijp}T_{jp}^{1*} + R_{ijpq}T_{jpq}^{2*} + g_{ikl}\varepsilon_{kl}^{0*} + g_{iklp}\varepsilon_{klp}^{1*} + g_{iklpq}\varepsilon_{klpq}^{2*}
\end{aligned}
\tag{11}
$$

where $\mathbf{D},\mathbf{R}$ and $\mathbf{g}$ are thermal, thermoelastic, and elastic Eshelby's tensors, respectively; the subscript $(.)_{,i'} = \partial x_i'$ represents partial derivative with respect to x_i'. Notice that when the source and field points are located in the different phases, $(.)_{,i'} = -(.)_{,i}$ holds. However, when source and points are located in the same phase, due to the existence of image terms, $(.)_{,i'} = -Q_I(.)_{,i}$ holds for image terms but $(.)_{,i'} = -(.)_{,i}$ works for original terms, i.e ϕ Eq. (3) of case $x_2'x_2 \geq 0$. Following conventional notations, the domain integral of potential functions are expressed through Greek capital letters,

$$
\begin{aligned}
\boldsymbol{\Phi}_{pq\ldots} &= \int_\Omega \phi(x_p'-x_p^c)(x_q'-x_q^c)\ldots d\mathbf{x}', \\
\boldsymbol{\Psi}_{pq\ldots} &= \int_\Omega \psi(x_p'-x_p^c)(x_q'-x_q^c)\ldots d\mathbf{x}' \\
\boldsymbol{\Theta}^y_{pq\ldots} &= \int_\Omega \alpha^y\phi(x_p'-x_p^c)(x_q'-x_q^c)\ldots d\mathbf{x}', \\
\boldsymbol{\Lambda}^y_{pq\ldots} &= \int_\Omega \beta^y\phi(x_p'-x_p^c)(x_q'-x_q^c)\ldots d\mathbf{x}'
\end{aligned}
\tag{12}
$$

where domain integrals $\boldsymbol{\Phi}_{pq}$ and $\boldsymbol{\Psi}_{pq}$ are available in Wu and Yin (2021a). Their image terms can be straightforwardly calculated by mirroring the cross-section without changing formulae. For instance, $\overline{\boldsymbol{\Phi}}_p(\mathbf{x},\mathbf{x}') = Q_P\boldsymbol{\Phi}_p(\mathbf{x},\overline{\mathbf{x}}')$ and its partial derivative $\overline{\boldsymbol{\Phi}}_{p,i'}(\mathbf{x},\mathbf{x}') = -Q_I\overline{\boldsymbol{\Phi}}_{p,i}(\mathbf{x},\mathbf{x}') = -Q_PQ_I\boldsymbol{\Phi}_{p,i}(\mathbf{x},\overline{\mathbf{x}}')$, which are elaborated in Appendix A.1. In the following, this section aims to provide closed-form formulae on four branches of $\boldsymbol{\Theta}$ and $\boldsymbol{\Lambda}$.

3.1. Definition of transformed coordinate (TC)

Consider an N_F sided arbitrary polygonal cross-section embedded in the bi-material domain D. As mentioned in Section 2, the bi-material interface S is assumed as plane $x_1 - x_2$ with $x_2 \equiv 0$, and the polygonal cross-section lies in exactly the same plane. Considering the lengthy formulae in Cartesian coordinates, alternatively, orthogonal transformed coordinates (TCs) are introduced to handle complex expressions on distances between vertices and field points. Shown in Fig. 2, TCs are constructed at each edge of the polygon through two normal unit vectors. For instance, the fth TC relies on the unit directional η_f^0 and outward normal λ_f^0 vectors, where vertices are aligned in counterclockwise sequences. Let m and n denote the first and second components of the fth unit directional vector η_f^0, and thus one can obtain $\lambda_f^0 = (n,-m)$ based on the orthogonal property of vectors. Based on TCs, the distances b_f and $l_f^\pm$ can be expressed as Eq. (13),

$$
b_f = \Big[(v_f^+)_i - x_i\Big](\lambda_f^0)_i, \quad l_f^\pm = \Big[(v_f^\pm)_i - x_i\Big](\eta_f^0)_i
\tag{13}
$$

where b_f is the perpendicular distance with respect to the fth edge and $l_f^\pm$ are horizontal distances defined in the fth TCs. During the partial differentiation process to obtain Eshelby's tensor, the area integrals can be converted to contour integrals. Despite source points within the cross-section, only points along the edges are of interest. Let $\eta = (x_i'-x_i)(\eta_f^0)_i$ denote the position of $\mathbf{x}'$ on the fth edge., the Galerkin's distance vector can be written as Eq. (14),

$$
x_i'-x_i = b_f(\lambda_f^0)_i + \eta(\eta_f^0)_i = \begin{cases} b_fn+\eta m & i=1 \\ -b_fm+\eta n & i=2 \end{cases}
\tag{14}
$$

3.2. Domain integrals of uniform potential functions

Eq. (8) shows that $\alpha^u = -\alpha^l$, $\overline{\alpha}^u = -\overline{\alpha}^l$ and $\overline{\alpha^u}(\mathbf{x},\mathbf{x}') = \alpha^u(\mathbf{x},\overline{\mathbf{x}}')$, and similar cases can be observed in Eq. (9) as well. Therefore, four

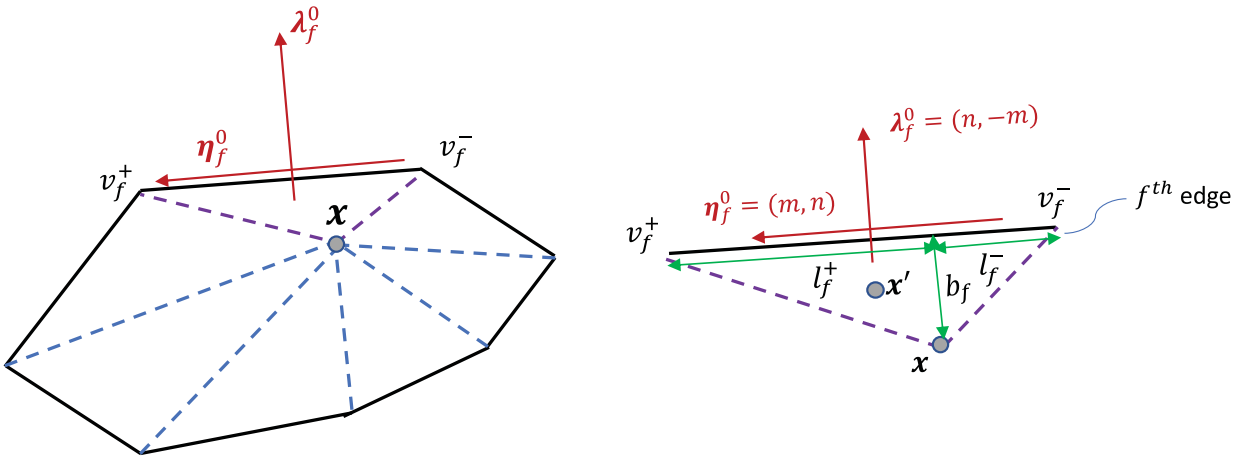

Fig. 2. Schematic plot of transformed coordinate (TC) on a N_F sided polygonal section.

branches of domain integrals can be derived from one branch, and the other three can be acquired through mirroring the cross-section, which is elaborated in Appendix A.2. Without the loss of any generality, this section mainly focuses on Θ^u and Λ^u. Using the Eq. (4) in Wu and Yin (2021a), domain integrals can be obtained,

$$\begin{aligned}
\Theta^u &= \sum_{f=1}^{N_F} \int_{\theta^-}^{\theta^+} \int_0^{b_f\sqrt{1+\tan^2[\theta]}} \rho \left\{ 2r_1 \arctan\left[\frac{r_1}{r_2}\right] + r_2(2 - \ln[\rho^2]) \right\} d\rho\, d\theta \\
&= \sum_{f=1}^{N_F} \mathcal{T}(b_f, l_f^+) - \mathcal{T}(b_f, l_f^-) \\
\Lambda^u &= \sum_{f=1}^{N_F} \int_{\theta^-}^{\theta^+} \int_0^{b_f\sqrt{1+\tan^2[\theta]}} \frac{\rho}{2} \left(4r_1 r_2 \arctan\left[\frac{r_1}{r_2}\right] \right. \\
&\quad \left. + (r_2^2 - r_1^2)(3 - \ln[p^2]) \right) d\rho\, d\theta \\
&= \sum_{f=1}^{N_F} \mathcal{L}(b_f, l_f^+) - \mathcal{L}(b_f, l_f^-)
\end{aligned} \tag{15}$$

where $r_1 = \rho\cos(\theta)n + \rho\sin(\theta)m$ and $r_2 = -\rho\cos(\theta)m + \rho\sin(\theta)n$; $\theta^\pm = \arctan[l_f^\pm / b_f]$ are integral limits of angle. And two functions $\mathcal{T}(b,l)$ and $\mathcal{L}(b,l)$ are provided as follows,

$$\begin{aligned}
\mathcal{T}(b,l) &= \frac{b}{18} \left\{ 12b^2 m \arctan\left[\frac{l}{b}\right] + 6((b^2+l^2)m + 2bln) \arctan\left[\frac{bn+lm}{-bm+ln}\right] \right. \\
&\quad \left. - ((b^2+l^2)n - 2blm)(3\ln[b^2+l^2] - 11) + 6b^2 n \ln[b^2+l^2] \right\} \\
\mathcal{L}(b,l) &= \frac{-b}{144} \left\{ 25\left[6b(b^2+l^2)mn + l(m^2-n^2)(l^2-3b^2)\right] \right. \\
&\quad + 12\left(4b^3(m^2-n^2) \arctan\left[\frac{l}{b}\right] \right. \\
&\quad \left. \left. + \left(3b(b^2+l^2)(m^2-n^2) + 2lmn(3b^2-l^2)\right) \arctan\left[\frac{bn+lm}{-bm+ln}\right] \right) \right. \\
&\quad \left. + 6\left(2bmn(b^2-3l^2) + l(3b^2-l^2)(m^2-n^2)\right) \ln\left[1 + \frac{l^2}{b^2}\right] \right\}
\end{aligned} \tag{16}$$

Shown in Eq. (11), the displacement field can be obtained through partial derivatives of potential functions, making it possible to apply Green's theorem possible. Hence, domain integrals on uniform potentials α^u and β^u are transformed into contour integrals,

$$\begin{aligned}
\Theta^u_{,i} &= -\sum_{f=1}^{N_F} (\lambda_f^0)_i \left(\mathcal{M}(b_f, l_f^+) - \mathcal{M}(b_f, l_f^-) \right) \\
\Lambda^u_{,i} &= -\sum_{f=1}^{N_F} (\lambda_f^0)_i \left(\mathcal{N}(b_f, l_f^+) - \mathcal{N}(b_f, l_f^-) \right)
\end{aligned} \tag{17}$$

where two integration functions $\mathcal{M}(b,l)$ and $\mathcal{N}(b,l)$ are provided as below (constant parts are separated),

$$\begin{aligned}
\mathcal{M}(b,l) &= \int 2(bn+\eta m) \arctan\left[\frac{bn+\eta m}{-bm+\eta n}\right] \\
&\quad + (-bm+\eta n)(2 - \ln[b^2+\eta^2])\, d\eta \\
&= \frac{3}{2} l(-2bm+ln) + b^2 m \arctan\left[\frac{l}{b}\right] \\
&\quad + l(2bn+lm) \arctan\left[\frac{bn+lm}{-bm+ln}\right] \\
&\quad + \frac{1}{2}(2blm + n(b^2-l^2)) \ln[b^2+l^2] \\
\mathcal{N}(b,l) &= \frac{1}{2} \int 4(bn+\eta m)(-bm+\eta n) \arctan\left[\frac{bn+\eta m}{-bm+\eta n}\right] \\
&\quad + \left((-bm+\eta n)^2 - (bn+\eta m)^2\right)(3 - \ln[b^2+\eta^2])\, d\eta \\
&= \frac{1}{18} \left\{ 11l\left(-6blmn + (m^2-n^2)(3b^2-l^2)\right) \right. \\
&\quad - 6b^3(m^2-n^2) \arctan\left[\frac{l}{b}\right] \\
&\quad + 6l\left(2mn(l^2-3b^2) - 3bl(m^2-n^2)\right) \arctan\left[\frac{bn+lm}{-bm+ln}\right] \\
&\quad \left. + 3\left(2bmn(3l^2-2b^2) + l(m^2-n^2)(l^2-3b^2)\right) \ln[b^2+l^2] \right\}
\end{aligned} \tag{18}$$

3.3. Domain integrals of linear and quadratic potential functions

Taking advantage of Galerkin's distance vector, source terms x'_p expanded at point x_p^c can be expressed in terms of Eq. (14) and field terms that $x'_p - x_p^c = (b_f(\lambda_f^0)_p + \eta(\xi_f^0)_p) + (x_p - x_p^c)$. Hence, and the first order partial derivative of Θ^u_p and Λ^u_p can be expressed as,

$$\begin{aligned}
\Theta^u_{p,i} &= \delta_{ip}\Theta^u + (x_p - x_p^c)\Theta^u_{,i} - \sum_{f=1}^{N_F} (\lambda_f^0)_i \left\{ (\lambda_f^0)_p b_f \left(\mathcal{M}(b_f, l_f^+) - \mathcal{M}(b_f, l_f^-) \right) \right. \\
&\quad \left. + (\xi_f^0)_p \left(\mathcal{M}^I(b_f, l_f^+) - \mathcal{M}^I(b_f, l_f^-) \right) \right\}
\end{aligned}$$

$$\Lambda^u_{p,i} = \delta_{ip}\Lambda^u + (x_p - x^c_p)\Lambda^u_{,i} - \sum_{f=1}^{N_F}(\lambda^0_f)_i \Big\{ (\lambda^0_f)_p b_f \Big(\mathcal{N}(b_f, l^+_f) - \mathcal{N}(b_f, l^-_f)\Big) + (\xi^0_f)_p \Big(\mathcal{N}^I(b_f, l^+_f) - \mathcal{N}^I(b_f, l^-_f)\Big) \Big\} \tag{19}$$

where two linear integration functions $\mathcal{M}^I(b,l)$ and $\mathcal{N}^I(b,l)$ are provided as below,

$$\begin{aligned}
\mathcal{M}^I(b,l) = \frac{1}{18}\Big\{ & -6b^3 n \arctan\Big[\frac{l}{b}\Big] + l\Big(2n(3b^2+8l^2) - 21blm\Big) \\
& + 6l^2(2lm+3bn)\arctan\Big[\frac{bn+lm}{-bm+ln}\Big] \\
& + 3\Big(b^3 m + l^2(3bm-2ln)\Big)\ln[b^2+l^2]\Big\} \\
\mathcal{N}^I(b,l) = \frac{1}{144}\Big\{ & 24b^4 mn \arctan\Big[\frac{l}{b}\Big] \\
& + l\Big(-8mn(3b^2+41l^2) + 3l(m^2-n^2)(38b^2-21l^2)\Big) \\
& + 24l^2\Big(3mn(2b^2-l^2) + 4bl(m^2-n^2)\Big)\arctan\Big[\frac{bm+lm}{-bm+ln}\Big]\Big) \\
& + 6\Big(16bl^3 mn + (m^2-n^2)(3l^4 - 6b^2l^2 - b^4)\Big)\Big\}
\end{aligned} \tag{20}$$

Similarly, the quadratic source terms $x'_p x'_q$ can be expressed as $(x'_p - x_p)(x'_q - x_q) + x_p x'_q + x'_q x_p - x_p x_q$. The quadratic domain integrals can be obtained by combining the interchanging rules of source, field terms, and uniform, linear domain integrals. Taking $\Theta^u_{pq,i}$ as an example,

$$\begin{aligned}
\Theta^u_{pq,i} = & \Big((x_p - x^c_p)\Theta^u_{q,i} + (x_q - x^c_q)\Theta^u_{p,i} + \delta_{pi}\Theta^u_q + \delta_{qi}\Theta^u_p\Big) \\
& - \Big((x_p - x^c_p)(x_q - x^c_q)\Theta^u_{,i} + (\delta_{pi}(x_q - x^c_q) + \delta_{qi}(x_p - x^c_p))\Theta^u\Big) \\
& - \sum_{f=1}^{N_F}(\lambda^0_f)_i \Big\{ (\lambda^0_f)_p(\lambda^0_f)_q b^2_f \Big(\mathcal{M}(b_f, l^+_f) - \mathcal{M}(b_f, l^-_f)\Big) \\
& + b_f\big((\lambda^0_f)_p(\xi^0_f)_q + (\lambda^0_f)_q(\xi^0_f)_p\big)\Big(\mathcal{M}^I(b_f, l^+_f) - \mathcal{M}^I(b_f, l^-_f)\Big) \\
& + (\xi^0_f)_p(\xi^0_f)_q\Big(\mathcal{M}^{II}(b_f, l^+_f) - \mathcal{M}^{II}(b_f, l^-_f)\Big)\Big\}
\end{aligned} \tag{21}$$

Following the same fashion, quadratic domain integrals Λ^u_{pq} can be written in terms of integration functions $\mathcal{N}$, $\mathcal{N}^I$, and $\mathcal{N}^{II}$. And two quadratic integration functions $\mathcal{M}^{II}(b,l)$ and $\mathcal{N}^{II}(b,l)$ are provided as below,

$$\begin{aligned}
\mathcal{M}^{II}(b,l) = \frac{1}{72}\Big\{ & l\big(6b^2(2bm+ln) + l^2(45ln-52bm)\big) - 12b^4 m\arctan\Big[\frac{l}{b}\Big] \\
& + 12l^3(4bn+3lm)\arctan\Big[\frac{bn+lm}{-bm+ln}\Big] \\
& - 6\big(b^4 n + l^3(3ln-4bm)\big)\ln\big[b^2+l^2\big]\Big\} \\
\mathcal{N}^{II}(b,l) = \frac{1}{900}\Big\{ & 30b^5(m^2-n^2)\arctan\Big[\frac{l}{b}\Big] \\
& - l\Big(15blmn(2b^2+99l^2) - 2(m^2-n^2)\big(15b^4 - 230b^2l^2 + 153l^4\big)\Big) \\
& + 30l^3\Big(-5bm(3lm+4bn) + 3ln(4lm+5bn)\Big)\arctan\Big[\frac{bn+lm}{-bm+ln}\Big] \\
& + 30\Big(bmn(b^4+15l^4) - l^3(m^2-n^2)(5b^2-3l^2)\Big)\ln[b^2+l^2]\Big\}
\end{aligned} \tag{22}$$

3.4. Circular domain integrals

For domain integrals Φ and Ψ, Dyson (1891) first proposed formulae to handle integrals with various density functions in ellipsoids. Later, Mura (1987) presented special cases of ellipsoids, including the case that one axis is infinitely long. Since plenty of work has discussed the two integrals, this section does not repeat such contents. Regarding bi-material domain integrals, Walpole (1997) studied a spherical inclusion embedded in two-jointed half-spaces, and the author suggested interchanging integral sequences. Subsequently, Liu et al. (2015) and Wu et al. (2023b) completed all cases of Θ and Λ with polynomial source fields. Recently, Dang et al. (2019) investigated Eshelby's problems in a semi-infinite domain, where the analytical expressions are proposed as a combination of several modified functions. However, the length of formulae (Eqs. (36 - 38) in Dang et al. (2019)) makes it difficult to be utilized for programming purposes. Therefore, this section aims to provide compact and simplified circular domain integrals based on potential functions.

Following the definition of potential functions in Eqs. (8) and (9), the integration sequence of their domain integrals can be switched (taking Θ^u and Λ^u, for example),

$$\begin{aligned}
\Theta^u(\mathbf{x}) &= \int_\Omega \alpha^u(\mathbf{x},\mathbf{x}')d\mathbf{x}' = \int_{x_2}^{-\infty}\int_\Omega \phi\, d\mathbf{x}'\, dt = \int_{x_2}^{-\infty} \boldsymbol{\Phi}\, dt \\
\Lambda^u(\mathbf{x}) &= \int_\Omega \beta^u(\mathbf{x},\mathbf{x}')d\mathbf{x}' = \int_{x_2}^{-\infty}\int_\Omega \alpha^u\, d\mathbf{x}'\, dt = \int_{x_2}^{-\infty} \Theta^u\, dt
\end{aligned} \tag{23}$$

where only finite parts are retained as other constants vanish during the partial differentiation process, and such a method is applicable to potentials with polynomial source terms as well. Notice that the bi-material displacement potential functions exclude singularity; thus, only the exterior part of $\boldsymbol{\Phi}$ is applied. Let $\mathbf{x}^c$ denote the center of the circular cross-section, and explicit formulae of $\boldsymbol{\Phi}, \boldsymbol{\Phi}_p$ and $\boldsymbol{\Phi}_{pq}$ are provided as below,

$$\begin{aligned}
\boldsymbol{\Phi} &= -\pi a^2 \ln|\mathbf{x}-\mathbf{x}^c|^2, \quad \boldsymbol{\Phi}_{,p} = (x_p - x^c_p)\frac{\pi a^4}{2|\mathbf{x}-\mathbf{x}^c|^2} \\
\boldsymbol{\Phi}_{pq} &= \pi a^2\Big\{ (x_p - x^c_p)(x_q - x^c_q)\frac{a^4}{6|\mathbf{x}-\mathbf{x}^c|^4} \\
&\quad - \frac{a^2}{4}\delta_{pq}\Big(\ln|\mathbf{x}-\mathbf{x}^c|^2 + \frac{1}{2} + \frac{a^2}{3|\mathbf{x}-\mathbf{x}^c|^2}\Big)\Big\}
\end{aligned} \tag{24}$$

Uniform circular domain integrals

$$\Theta^s = \pi a^2 \alpha^s \qquad \Lambda^s = \pi a^2 \beta^s \tag{25}$$

Linear circular domain integrals

$$\Theta^s_p = \frac{\pi a^4}{4}\begin{cases} -\alpha^s_{,p} & p=1 \\ \phi^s & p=2 \end{cases} \quad \& \quad \Lambda^s_p = \frac{\pi a^4}{4}\begin{cases} -\beta^s_{,p} & p=1 \\ \alpha^s & p=2 \end{cases} \tag{26}$$

Quadratic circular domain integrals

$$\Theta^s_{pq} = \frac{\pi a^4}{24}\begin{cases} a^2\phi^s_{,2} + 3\gamma^s x_2 + 6\alpha^s & p,q \neq 2 \\ -a^2\phi^s_{,p} & p \neq 2, q = 2 \\ -a^2\phi^s_{,2} + 3\gamma^s x_2 + 6\alpha^s & p = q = 2 \end{cases} \quad \&$$

$$\Lambda^s_{pq} = \frac{\pi a^4}{24}\begin{cases} a^2\alpha^s_{,2} - \frac{3x_2^2}{2}\gamma^s + 6\beta^s & p,q \neq 2 \\ -a^2\alpha^s_{,p} & p \neq 2, q = 2 \\ -a^2\alpha^s_{,2} - \frac{3x_2^2}{2}\gamma^s + 6\beta^s & p = q = 2 \end{cases} \tag{27}$$

where the superscript s represents four branches of functions, which is up to positions of source and field points; $\gamma^s = 1$ when $s = u$ or $s = \overline{(.)}^l$ and $\gamma = -1$ when $s = \overline{(.)}^u$ and l. Their derivatives have been implemented in the package "POLYGON - EIM", which will be elaborated in Appendix B.

3.5. Discussion on singularity issues of polygonal domain integrals

Singularity is a fascinating topic when the source domain exhibits a non-smooth boundary. For ellipsoidal or elliptical inclusions in 3D and 2D, respectively, no singularity exists but discontinuities of the strain and temperature gradient field can be found (Mura, 1987). For polyhedral or polygonal inclusions, Rodin (1996) has demonstrated that for elastic inclusion problems with a uniform eigenstrain, a weak singularity of $\ln r$ or a strong singularity of $1/r$ exhibits for the strain field in the neighborhood of a vertex of a polygonal or a polyhedral inclusion, respectively. This paper extends Rodin's work to thermoelastic problem, but the singularity will follow the similar fashion.

Firstly, this paper considers a bi-material infinite domain. However, as long as the polygonal inclusion is within one material phase as we discussed in this paper, the same singularities retain as a single material infinite domain investigated by Rodin (1996). The reason is that the bi-material fundamental solutions are derived through superposition of infinite one and relevant image terms, original components of infinite fundamental solutions produce singularity issues at the vertices. However, the image terms exhibit a distance from the vertices but will not produce any singularity issue unless vertices are on the bi-material interface, which will be investigated in the future. Note that the vertex on the interface may generate a higher order singularity than an inner vertex does because both the interfacial discontinuity plays an additional role in the singularity. However, this paper limits to the inner vertex, which shall exhibit the same singularity as Rodin (1996) studied.

Secondly, this paper covers three Green's functions while Rodin studied the elastic case only (Rodin, 1996). The thermal Green's function shares the same singularity order as the elastic Green's function, as the harmonic potential plays the role. However, for thermal elastic problem, because the continuity of the thermoelastic Green's function is one order higher than the elastic Green's function, the strain field caused by a uniform heat source will not be singular anymore. Note that a temperature change in an inclusion produces an eigenstrain, which produces stress singularity as well.

Thirdly, this paper considers different types of sources beyond the uniform eigen-fields. Specifically, distributed heat sources and forces, polynomial eigen-temperature gradient (ETG), polynomial eigenstrain are considered. The strain field caused by uniformly distributed heat sources or forces exhibit continuity one order higher than the corresponding uniform eigen-fields, so the uniform eigen-fields play the controlling role on the overall singularity. Note that for a polynomial eigen-field with the reference point on the vertex, the uniform term plays the dominant role on singularity as the higher order-term provide low source intensity at the neighborhood of the vertex.

4. Numerical verification with circular inhomogeneity problem

The above-provided closed-form domain integrals can provide exact solutions to thermal and elastic fields of Eshelby's inclusion problems, where the eigen-fields are continuously distributed over the inclusion up to quadratic order. Besides the inclusion problem, the aforementioned domain integrals can be applied in Eshelby's equivalent inclusion method to investigate disturbance by the mismatch of material properties. Shown as Fig. 3, this section considers a circular subdomain with radius $a = 0.1$ m embedded in two jointed dissimilar half-spaces with distance $h = 1.2a$ to the bimaterial interface S. A line heat source $q = 10$ kW/m^3 and uniform far-field load $\sigma^0_{22} = -10$ kPa are applied to the system. Without the loss of any generality, (i) the upper phase D^+ exhibits 1 W/m K, 3 MPa, 0.2, 10 kPa, (ii) the lower phase D^- exhibits 10 W/m K, 1.5 MPa, 0.2, 20 kPa, and (iii) the inhomogeneity Ω exhibits 5 W/m K, 1 MPa, 0.3, 0 for thermal conductivity, shear modulus, Poisson's ratio, and thermal modulus, respectively. $3, 4, 12, 20-$, and $100-$ equal-sized regular polygons are employed to approximate the circular cross-section to conduct Eshelby's thermal and elastic EIM. In order to verify uniform, linear and quadratic domain integrals, the solutions are compared among finite element method (FEM), Eshelby's method with analytical circular and polygon-approximated integrals on thermal and elastic fields. The following subsection provides details on acquiring initial stress components in FEM, which is due to the non-uniformity of loads.

4.1. Finite element model and preparation for initial stress components

In this section, the FEM model is built upon the commercial software ANSYS with steady-state and static elastic functions. To reduce thermal boundary effects, shown in Fig. 4, (i) the dimension of bimaterial matrix are 20 m × 20 m; and (ii) uniform temperature boundary conditions −2.08 °C are setup with on the left, right, bottom and top edges, respectively. Regarding elastic boundary conditions, (i) the displacement components u_1 and u_2 are constrained for the left and bottom edge, respectively; (ii) the left bottom corner is constrained to avoid rigid body motion; (iii) the right edge is traction-free; and (iv) a 10 kPa uniform pressure is applied on the top edge (for an elastic stress test in Section 4.3, which is suppressed in Section 4.4). Unlike the infinite space, a uniform far-field load results in linear stress variation in the neighborhood of the bimaterial interface. Therefore, it is inappropriate to use uniform far-field strain/stress as initial conditions. Instead, the circular domain is first filled with the same material as the matrix, and the stress and its partial derivatives at the expansion center are obtained and applied as initial stress conditions for EIM. Based on FEM, (i) $\sigma^0_{11} = 1014.9$ Pa, $\sigma^0_{22} = -10.03$ kPa with linear slope $\sigma^0_{11,1} = 0, \sigma^0_{11,2} = -149.21$ Pa, $\sigma_{22,1} = 33.33$ Pa and $\sigma_{22,2} = 22.22$ Pa for the upper region near the interface; (ii) $\sigma^0_{11} = -736.92 + 100.66x_2$ Pa and $\sigma^0_{22} = -10027 + 22.22x_2$ Pa for the lower region near the interface, where (i) is applied as initial stress conditions for EIM.

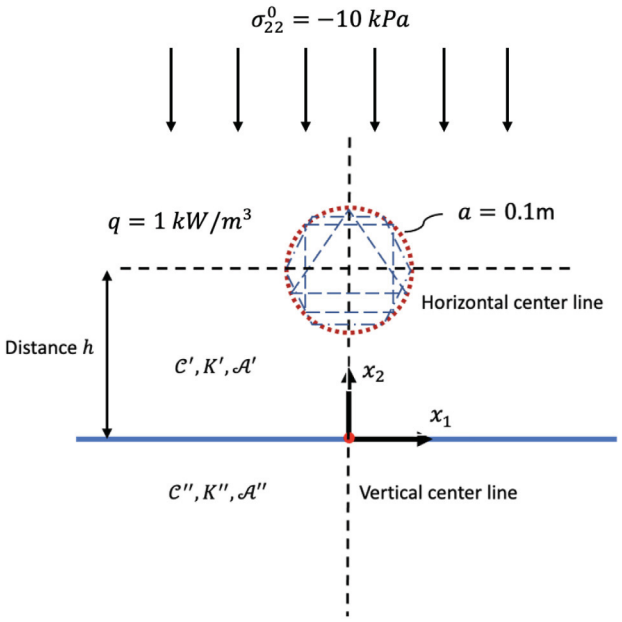

Fig. 3. One circular inhomogeneity (radius $a = 0.1$ m, heat source $q = 10$ kW/m^3) is subjected to far-field load $\sigma^0_{22} = -10$ kPa approximated by $3, 4, 12, 20$ and 100 edges embedded in a two jointed dissimilar half-spaces with distance h to the bimaterial interface.

4.2. Comparison of thermal fields among circular and non-circular approximated polygons

As indicated in Eq. (1), when the source and field points are in the same material phase, the fundamental solution contains both the original harmonic potential and its image term. This subsection aims to verify the appropriate handling of image terms in Appendix A.1. Shown in Fig. 5(a) and 5(b), the temperature and flux are compared between FEM and EIM with uniform, linear and quadratic ETGs. When the inhomogeneity is embedded in the infinite medium, a combination of uniform and linear ETG can provide the exact thermal solutions, which are elaborated in Section 5. However, since the circular inhomogeneity are placed close to the bimaterial interface S, the material mismatch of the two matrix results in a more complicated variation of thermal fields. Taking the above case, for instance, because the thermal conductivity significantly changes ($K' = 0.1K''$), the slope of temperature and flux

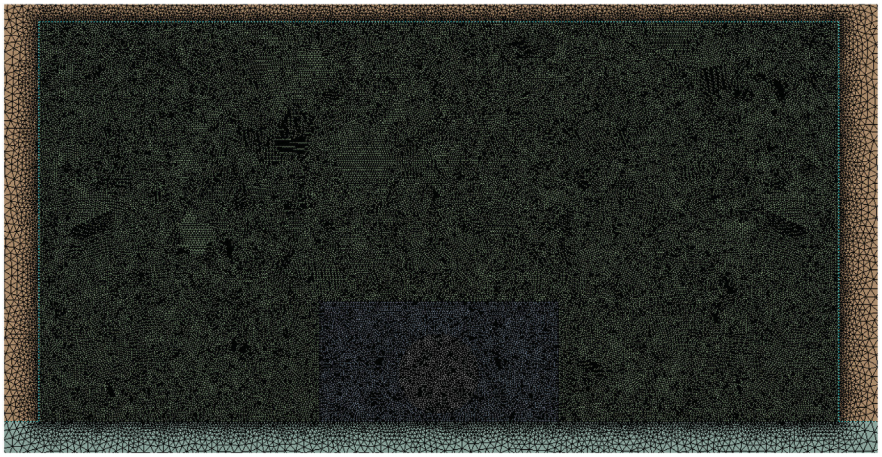

Fig. 4. Plot of FEM mesh for a circular inhomogeneity embedded in the two jointed dissimilar half-spaces; 0.005 m element size used in circular and its related two rectangles; 0.05 m element size used in two other larger rectangles.

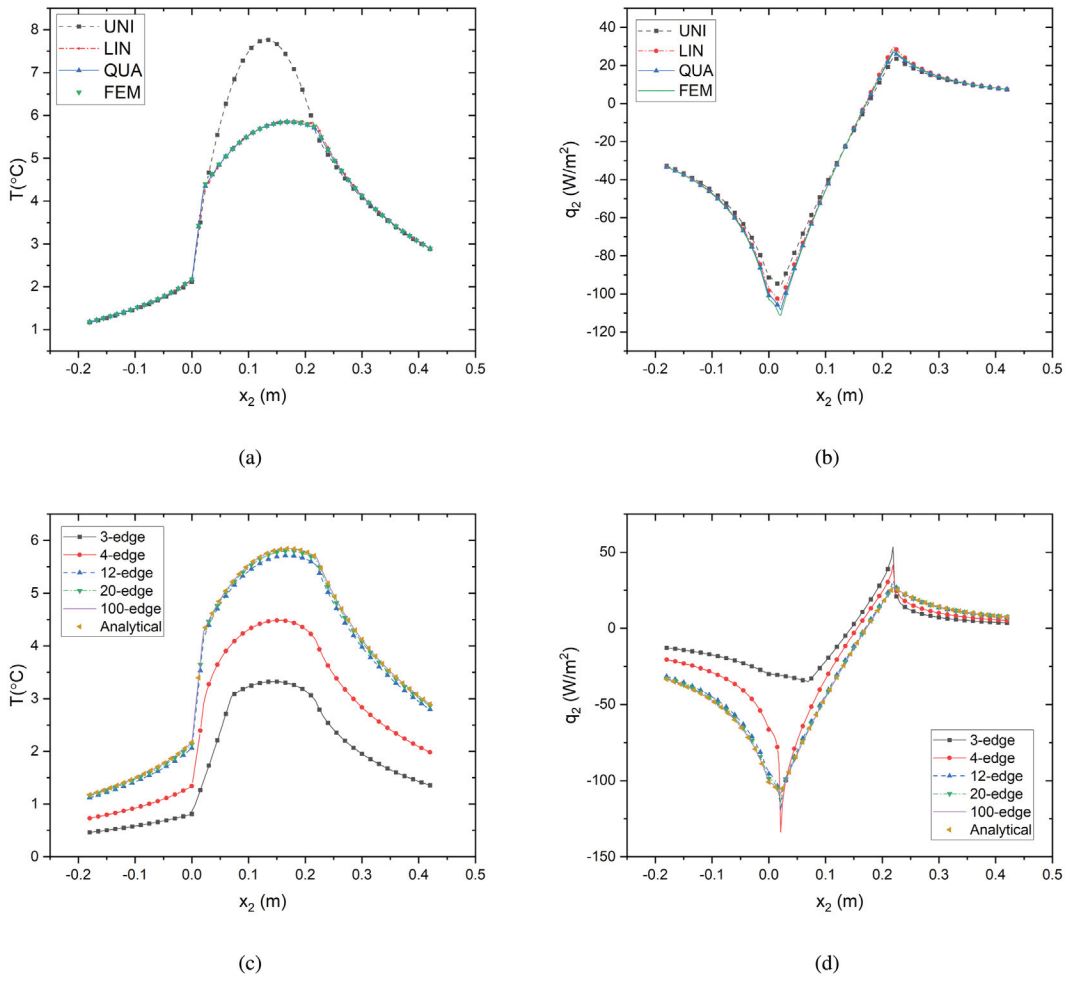

Fig. 5. Verification and comparison of thermal field between EIM and FEM along the vertical center line, (a) temperature T and (b) flux q_2 obtained by uniform, linear and quadratic ETG with analytical circular domain integrals; (c) temperature T and (d) flux q_2 obtained by $3, 4, 12, 20, 100-$ equal edged polygons with quadratic ETG.

changes accordingly to match continuity equations. In such a case, quadratic and actually even higher-order variations of flux are expected due to the interfacial effects. Fig. 5(b) verifies the higher order variation of flux, and EIM with quadratic ETG has the smallest discrepancies compared with that of uniform and linear ETGs. Fig. 5(c) and 5(d) compare temperature and flux calculated by domain integrals with five polygons. Since the circle is approximated by regular equal-edge polygons, more edges could better describe the geometric features. It is observed that $3, 4-$edged polygons can seldom catch the features which exhibit large discrepancies between the analytical solutions and other polygons. 12-edged polygons can provide close predictions, but the thermal fields show larger difference around the top and bottom.

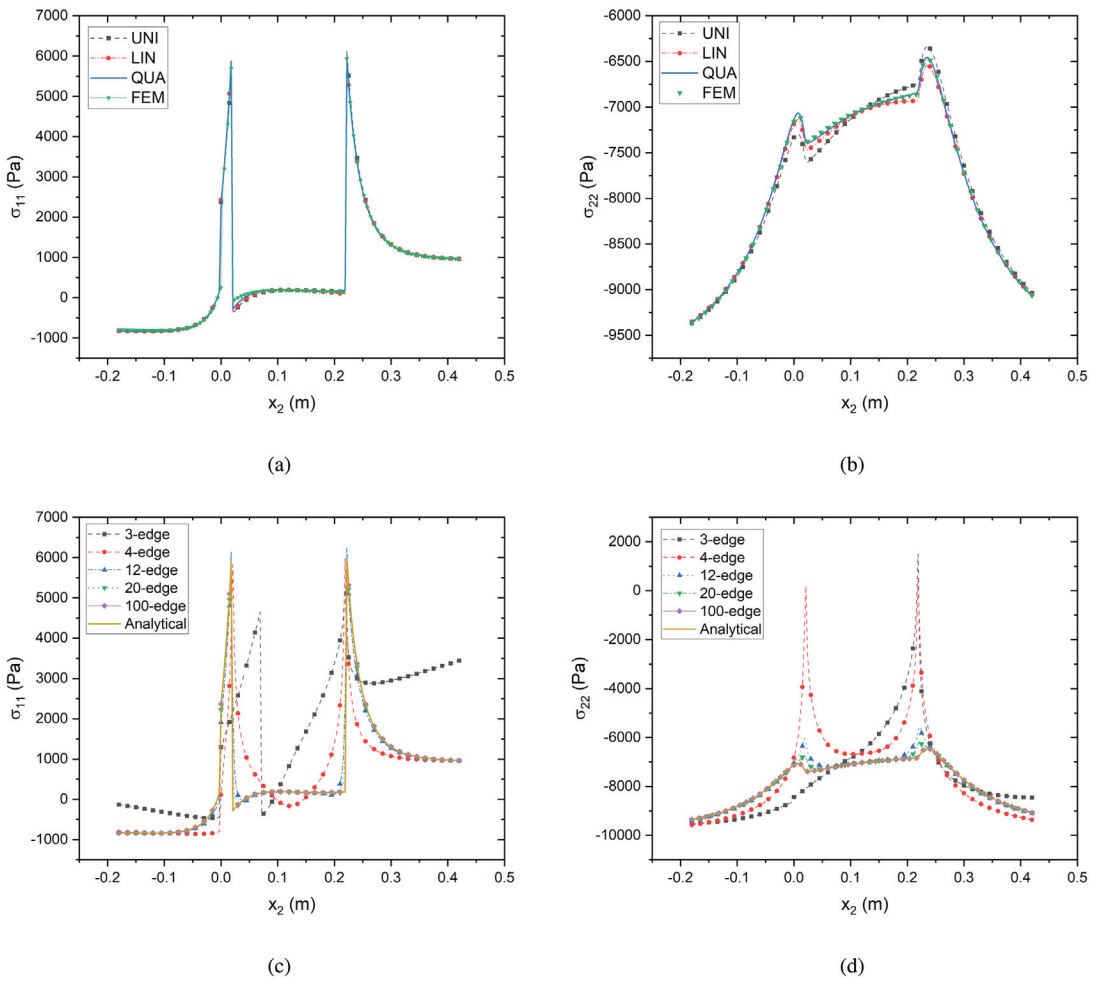

Fig. 6. Verification and comparison of stress fields between EIM and FEM along the vertical center line, (a) normal stress σ_{11} and (b) normal stress σ_{22} obtained by uniform, linear and quadratic eigenstrain with analytical circular domain integrals; (c) normal stress σ_{11} and (d) normal stress σ_{22} obtained by $3, 4, 12, 20, 100-$ equal edged polygons with quadratic eigenstrain.

When the number of edges increases, good comparisons can be found between the 100-edged polygon and the analytical solution.

4.3. Comparison of stress fields among circular and non-circular approximated polygons

This subsection verifies the domain integrals of Boussinesq's potentials. As mentioned in Section 4.1, this section set nil thermal modulus to obtain regular initial stress components for EIM. Following the same fashion, we first compared FEM and EIM with analytical circular domain integrals. Shown in Fig. 6(a) and 6(b), similar to thermal fields, EIM with quadratic exhibit the minor discrepancies compared to that of FEM. As a tribute to Eshelby's work, when the inhomogeneity is embedded in an infinite medium, the uniform representation of eigenstrain is the exact solution. Even for an inclusion problem, the mismatch of two matrix materials changes the order of load from uniform to linear. However, questions may arise that for linear initial stress fields, why do the elastic fields differ between the linear and quadratic eigenstrain? This question should be answered in aspects of fundamental solution as Eq. (3). We shall first the problem in an infinite space with Kelvin's solution, and a linear variation of the initial field can only result in a combination of uniform and linear eigenstrain. However, the bimaterial fundamental solution consists of Kelvin's solution and Boussinesq's displacement potentials. Unlike the harmonic, bi-harmonic functions, which yield zero at the center of expansion for higher order derivatives, i.e., uniform potentials are zero under 5th order derivatives, Boussinesq's displacement potentials still have influences. Therefore, equivalent stress conditions for quadratic terms are no longer zero, resulting in such differences. Fig. 6(c) and 6(d) compares solutions between analytical circular domain integrals and equal-edged polygon approximated solutions. When the number of edges increases, the results of an equal-edge polygon gradually recover the analytical solution except for the top and bottom vertices. In addition, the stress singularities caused by polygon vertices vanish rapidly for both interior and exterior parts. Except for the cases of 3 and 4 edge, other cases with $12, 20, 100$ can provide good agreement with analytical domain integrals, which can be further applied for elastic analysis of other geometries.

4.4. Comparison of thermoelastic stress fields among circular and non-circular approximated polygons

Although the thermoelastic field by a circular heat source may not vary as much as the elastic stress fields, there are constant stresses between FEM and DEIM results due to BCs. For readers' reproduction, $\sigma_{11}^0 = -2.32$ kPa and $\sigma_{22}^0 = -15.03$ kPa are used in verification of DEIM, which are obtained in a similar way as elastic one through inclusion problem. Fig. 7(a) compares FEM and DEIM with uniform, linear and quadratic eigen-fields and the same conclusion can be drawn that quadratic eigen-fields can better approximate the actual fields. Since the thermoelastic solutions are the superposition of thermal and elastic parts, the discrepancies from temperature accumulates, which results

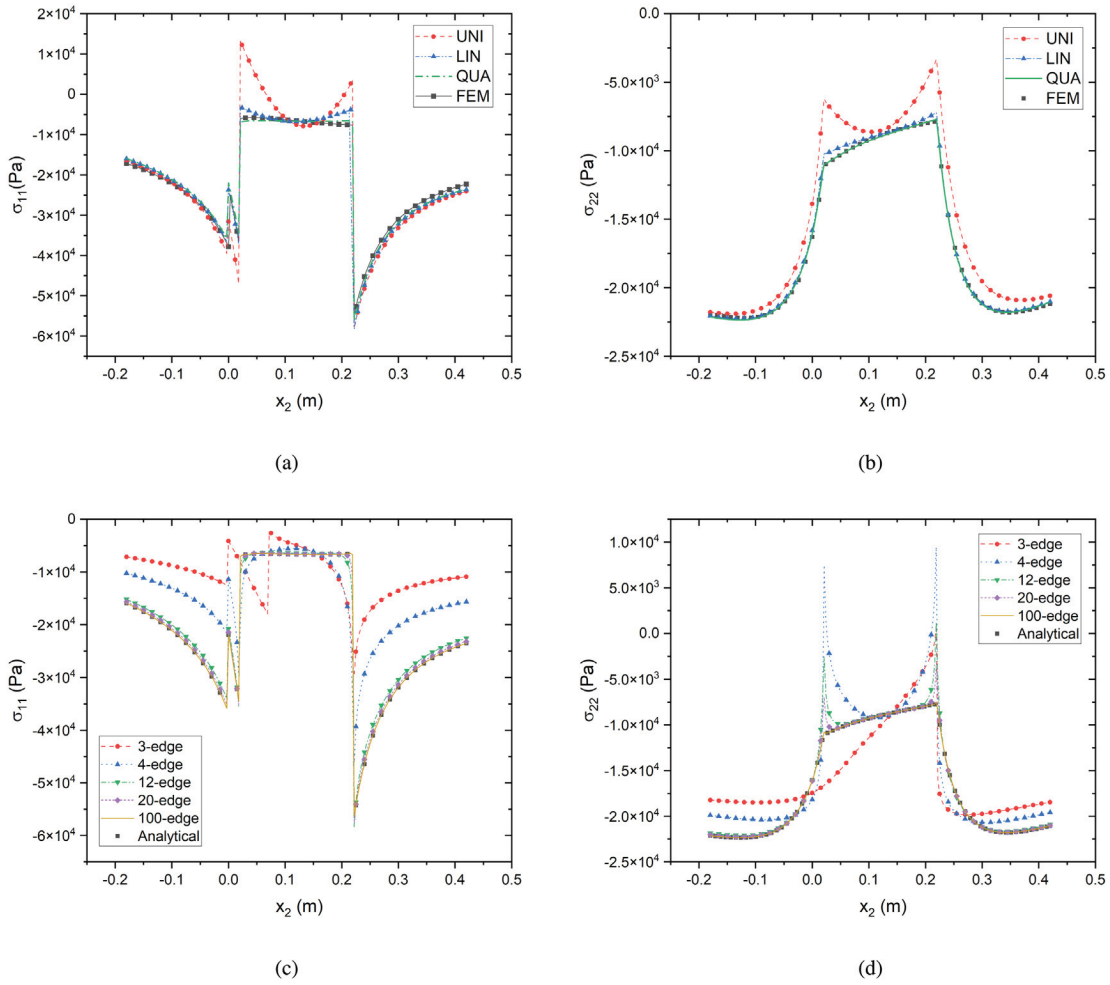

Fig. 7. Verification and comparison of stress fields between DEIM and FEM along the vertical center line, (a) normal stress σ_{11} and (b) normal stress σ_{22} obtained by uniform, linear and quadratic eigenstrain with analytical circular domain integrals; (c) normal stress σ_{11} and (d) normal stress σ_{22} obtained by $3, 4, 12, 20, 100-$ equal edged polygons with quadratic eigenstrain.

in much larger discrepancies in elastic stress compared to Fig. 6(b). Fig. 7(b) shows similar trends, and the application of linear eigen-fields significantly improves approximation accuracy. The reason is that a uniform ETG cannot accurately describe thermal fields, and even for an infinite medium (in the next section), we show that a linear ETG is an exact solution where no uniform ETG is necessary. Fig. 7(c) and 7(d) apply polygons to approximate the circle. Given a low number N_F, their main difference exists in the neighborhood of top and bottom vertices, which require more edges to capture the geometry.

5. Case study of an electric cable with different cross section in a large concrete block

The previous section verifies domain integrals of arbitrarily shaped polygons through comparison with FEM and analytical solution. The section aims to derive the analytical thermal, thermoelastic solution of a single circular inhomogeneity with a prescribed uniform heat source embedded in an infinite space. A typical application of such a case is the analysis of an electric cable embedded in a concrete block.

5.1. Dual equivalent inclusion method

In our recent work (Wu et al., 2023a), the DEIM is proposed to handle trivial procedures to couple the thermoelastic analysis. Using the technique of Green's function, DEIM avoids volume integrals of temperature over the entire domain by limiting it within inhomogeneities. Although tedious to duplicate Eq. (28) in Wu et al. (2023a), it is of importance to list the equation as Eq. (28),

$$\begin{aligned}
&C^w_{ijkl}(\varepsilon^\infty_{kl}+\varepsilon'_{kl}+\varepsilon^Q_{kl}+\varepsilon^E_{kl}-\varepsilon^{I0*}_{kl})-\mathcal{A}^w\delta_{ij}\Delta T\\
&\quad=C^I_{ijkl}(\varepsilon^\infty_{kl}+\varepsilon'_{kl}+\varepsilon^Q_{kl}+\varepsilon^E_{kl})-\mathcal{A}^I\delta_{ij}\Delta T\\
&C^w_{ijkl}(\varepsilon^\infty_{kl,m}+\varepsilon'_{kl,m}+\varepsilon^Q_{kl,m}+\varepsilon^E_{kl,m}-\varepsilon^{I1*}_{klm})-\mathcal{A}^w\delta_{ij}\Delta T_{,m}\\
&\quad=C^I_{ijkl}(\varepsilon^\infty_{kl}+\varepsilon'_{kl}+\varepsilon^Q_{kl}+\varepsilon^E_{kl})_{,m}-\mathcal{A}^I\delta_{ij}\Delta T_{,m}\\
&C^w_{ijkl}(\varepsilon^\infty_{kl,mn}+\varepsilon'_{kl,mn}+\varepsilon^Q_{kl,mn}+\varepsilon^E_{kl,mn}-2\varepsilon^{I2*}_{klmn})-\mathcal{A}^w\delta_{ij}\Delta T_{,mn}\\
&\quad=C^I_{ijkl}(\varepsilon^\infty_{kl}+\varepsilon'_{kl}+\varepsilon^Q_{kl}+\varepsilon^E_{kl})_{,mn}-\mathcal{A}^I\delta_{ij}\Delta T_{,mn}
\end{aligned}\tag{28}$$

where $\varepsilon^\infty_{ij}, \varepsilon'_{ij}, \varepsilon^*_{ij}$ are initial far-field strain, disturbed strain (by eigenstrain) and eigenstrain, respectively; ε^Q_{ij} and ε^E_{ij} are disturbed strain caused by the heat source and ETG, respectively. For a linear problem, the disturbed strain by eigenstrain, heat source, and ETG can be obtained by applying compatibility law on Eq. (11). The ETG are determined through thermal equivalent flux equations, and readers can refer to Eq. (15) in Wang et al. (2022).

5.2. Exact thermoelastic solution of an circular inhomogeneity embedded in an infinite domain

Consider a constant heat source q^v distributed within the circular subdomain Ω with K^I located at the origin point, where the reference temperature is assumed at the center of inhomogeneity. Through

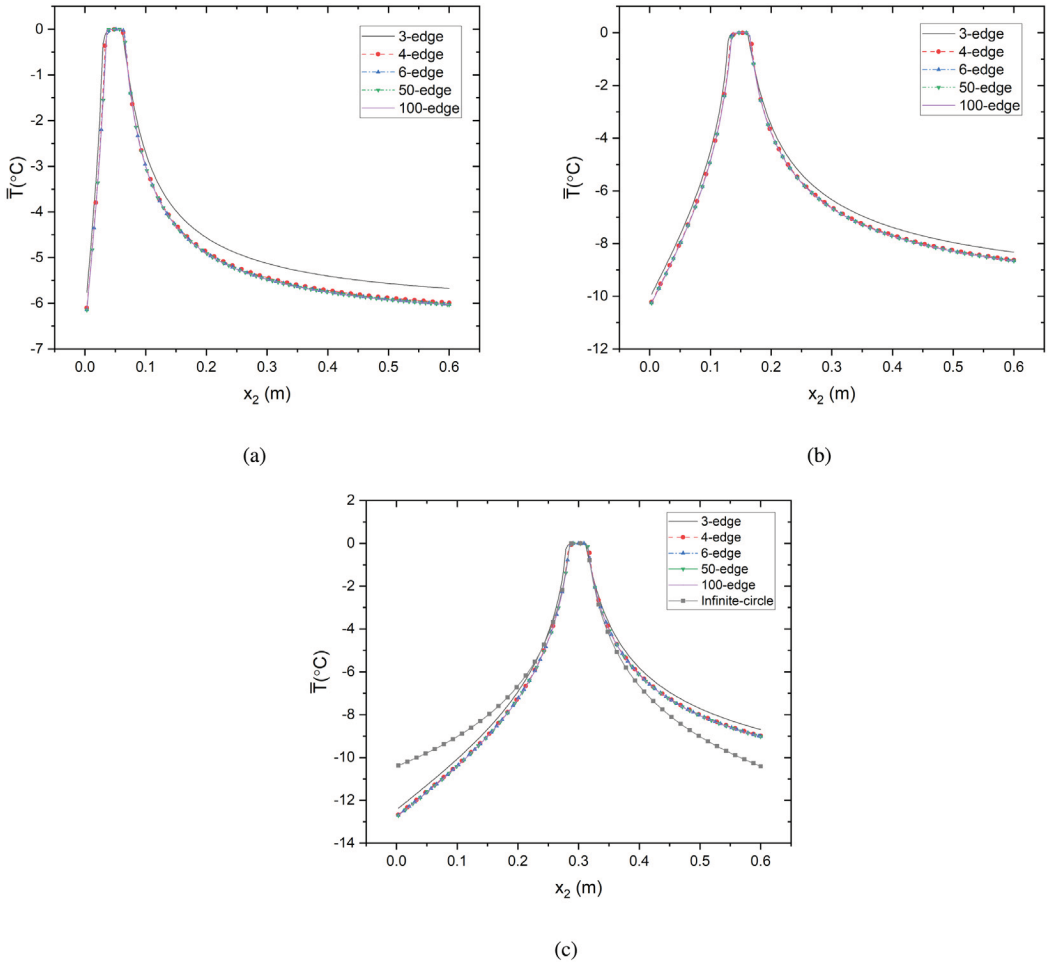

Fig. 8. Variation of temperature $\overline{T}$ along x_2 within $[0.003, 0.6]$ m when electric cable is located at different height, (a) 0.05 m, (b) 0.15 m and (c) 0.30 m (in comparison to Eq. (29)).

thermal equivalent flux conditions, a linear ETG can be obtained as Eq. (29),

$$T^*_{ij} = \frac{K - K^I}{-2KK^I} q_v \delta_{ij} \tag{29}$$

then the temperature is,

$$\begin{aligned} T(\mathbf{x}) &= \frac{q_v}{4\pi K}\left\{\boldsymbol{\Phi} + \frac{K-K^I}{2K^I}\boldsymbol{\Phi}_{i,i}\right\} \\ &= \frac{q_v}{4K}\begin{cases} (1-\ln a^2)a^2 + \frac{K-K^I}{K^I}a^2 - \frac{K}{K^I}|x|^2 & |x| \le a \\ -a^2 \ln |x|^2 & |x| > a \end{cases} \end{aligned} \tag{30}$$

$$\boldsymbol{\Phi}(\mathbf{x}) = \pi \begin{cases} a^2(1-\ln a^2) - |x|^2 & |x| \le a \\ -a^2 \ln |x|^2 & |x| > a \end{cases} \tag{31}$$

where the contribution of linear ETG vanishes for exterior field points; $\boldsymbol{\Phi}$ is first presented considering the constant of the interior part, which is often neglected by the community in the partial differentiation process. Through solving Eq. (28), the eigenstrain can be obtained as the combination of uniform and quadratic terms as Eq. (32),

$$\varepsilon^*_{ij}(\mathbf{x}) = \overline{\varepsilon}^H \delta_{ij} + (\overline{\varepsilon}^A \delta_{ij}\delta_{mn} + \overline{\varepsilon}^B(\delta_{im}\delta_{jn} + \delta_{in}\delta_{jm}))(x_m - x^c_m)(x_n - x^c_n) \quad |x| \le a \tag{32}$$

where components of uniform and quadratic eigenstrain are,

$$\begin{aligned} \overline{\varepsilon}^A &= \frac{q_v}{S}(\mathcal{A} - \mathcal{A}^I)(\mu + (3-4\nu)\mu^I) \\ &\quad - 2\mathcal{A}(1-2\nu)\left(\mu(\lambda + \mu - 2\lambda^I) + (\lambda - \mu)\mu^I\right) \\ \overline{\varepsilon}^B &= -\frac{q_v}{S}(\mu - \mu^I)(\mathcal{A}^I + \mathcal{A}) \quad \& \\ S &= 16K^I\left((1-2\nu)(\lambda+\mu)\mu^I + (\lambda^I + \mu^I)\mu\right) \end{aligned} \tag{33}$$

and see equation in Box I.

By using Eq. (11) with elastic and thermoelastic Eshelby's tensors, the displacement can be obtained,

$$\begin{aligned} u_i(\mathbf{x}) &= \frac{1}{8\pi(1-\nu)}\left\{ \frac{\alpha(1+\nu)q_v}{K}\left[\Psi_{,i} + \frac{K-K^I}{2K^I}\Psi_{m,im}\right] + \overline{\varepsilon^H}[\Psi_{,imm} - 4\Phi_{,i}] \right. \\ &\quad \left. + \overline{\varepsilon^A}[\Psi_{mm,ihh} - 4\Phi_{mm,i}] + 2\overline{\varepsilon^B}[\Psi_{mh,imh} - 2\nu\Phi_{mm,i} - 8(1-\nu)\Phi_{im,m}] \right\} \\ &= \frac{x_i}{8(1-\nu)}\begin{cases} \alpha(1+\nu)q_v\left[\frac{(2K-K^I)}{2K}(2a^2 - |x|^2) - a^2\ln(a^2)\right] + 4\overline{\varepsilon}^H \\ \quad + 2|x|^2\overline{\varepsilon}^A + [2(-3+4\nu)a^2 + (9-10\nu)|x|^2]\overline{\varepsilon}^B & |x| \le a \\ \frac{a^2\alpha(1+\nu)q_v}{4}\left[\frac{a^2(K-3K^I)}{K|x|^2} - 8\ln|x|^2\right] & \\ \quad + 8\frac{a^2}{|x|^2}\overline{\varepsilon}^H + \frac{2a^4}{|x|^2}(1-\nu)\overline{\varepsilon}^B & |x| > a \end{cases} \end{aligned} \tag{35}$$

where $\alpha = \mathcal{A}/(3\lambda + 2\mu)$ denotes the thermal expansion coefficient.

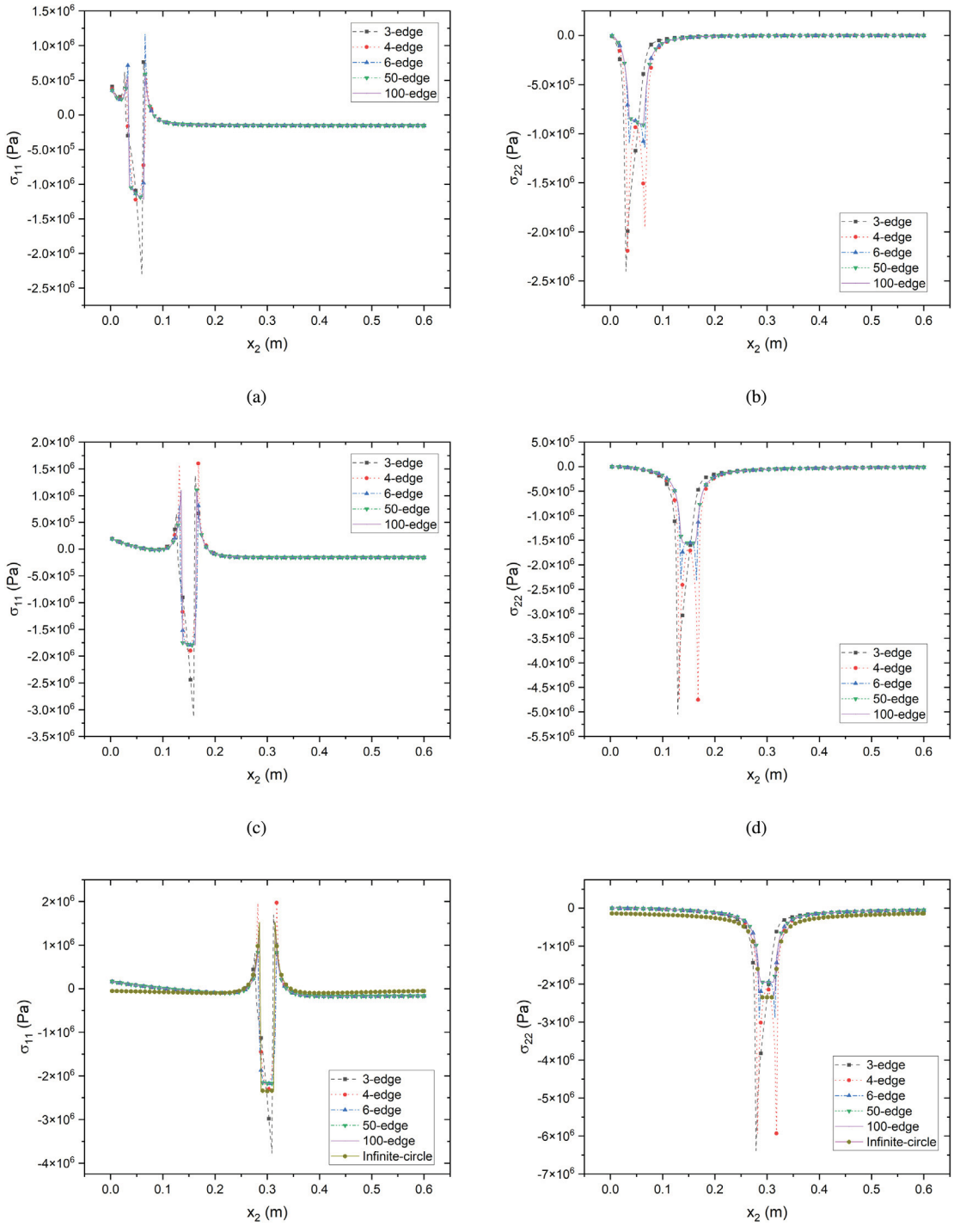

Fig. 9. Variation of normal stresses along x_2 axis within $[0.003, 0.06]$ m when the polygonal cross-section is located at three distances, (a) σ_{11}, (b) σ_{22} for $h = 0.05$ m; (c) σ_{11}, (d) σ_{22} for $h = 0.15$ m; (e) σ_{11}, (f) σ_{22} for $h = 0.30$ m.

Note that one can similarly derive the exact thermoelastic solution of spherical inhomogeneity embedded in an infinite space for the 3D problem (see Section 6.1 in Wu et al. (2023a)).

5.3. *Comparison of temperature and thermoelastic fields among circular and non-circular approximated polygons*

Considering an electric cable with a polygonal cross-section embedded in a large concrete block, it usually generates heat, which causes thermal stresses in the concrete phase. Because the concrete block is much larger than the cross-section of the cable, the problem can be simplified as a semi-infinite one, where concrete and air serve as the upper and lower phase, respectively. As shown in Eqs. (1)–(3), the interfacial effects decrease with the increasing distance ratios (h/a), where a is the characteristic dimension of the cross-section. Hence, to investigate both geometries, polygons with N_F wedges ($N = 3, 4, 6, 50, 100$) with the same cross-section area (6.4516 cm^2) and heat

$$\bar{\varepsilon}^H = a^2 q_v \frac{K\Big((\mathcal{A}^I-\mathcal{A})\Big[\mu\big[(1-2\nu)(\lambda+\mu)+(3-2\nu)\lambda^I\big]+\mu^I(1-2\nu)\big[(3-4\nu)\lambda+\lambda^I+\mu^I\big]+2(3-6\nu+4\nu^2)\mu\mu^I\Big]\Big)+\mathcal{A}(1-2\nu)\mu^{-1}\big[\lambda+\mu-\lambda^I-\mu^I\big]\big[(1-2\nu)\lambda(\mu+\mu^I)+\mu\big(2\lambda^I+(1-2\nu)\mu+(3-2\nu)\mu^I\big)\big]-4K^I\ln(a)\Big[2(\mathcal{A}^I-\mathcal{A})(1-\nu)+\mathcal{A}(1-2\nu)\mu^{-1}\big[\lambda+\mu-\lambda^I-\mu^I\big]\big[\mu(\lambda^I+\mu^I)+\mu^I(1-2\nu)(\lambda+\mu)\big]\Big]}{SK\big(\lambda^I+\mu^I+(1-2\nu)(\lambda+\mu)\big)} \tag{34}$$

Box I.

generation rate 33 kW/m^2 are applied. Regarding the distance effects, they are placed with $h = 0.05, 0.15$, and 0.30m below the interface. The material properties are selected as, (i) $K' = 1$ W/m K, $\mu' = 1.5$ GPa, $\nu' = 0.2$ and $\mathcal{A}' = 60$ kPa for the concrete; (ii) $K'' = \infty$, $\mu'' = \nu'' = \mathcal{A}'' = 0$ for the air to create the constant temperature interfacial condition; and (iii) $K^I = 237$ W/m K, $\mu^I = 26.25$ GPa, $\nu^I = 0.33$ and $\mathcal{A}^I = 8.453$ MPa for the cable.

Fig. 8(a–c) compare temperature $\overline{T} = T(\mathbf{x}) - T(\mathbf{x}^c)$ along x_2 axis among polygonal cross-section with $3, 4, 6, 50$ and 100 edges. It is observed that the temperature of the $3-edge$ polygon exhibits different trends, which are caused by different center temperatures. As for other cases, although they exhibit some discrepancies within the cross-section, the differences vanish rapidly. When the distance h decreases, the two end-point temperatures increase, and their differences become larger as the interfacial effects become intensive. Since the dominant function of temperature is $\ln r$, the interfacial effects require larger distances to vanish. As indicated in Fig. 8(c), when comparing temperatures with the solution in Eq. (29) (center at 0.3 m), apparent discrepancies are observed around two end-points.

Fig. 9(a–e) compare temperature $\overline{T} = T(\mathbf{x}) - T(\mathbf{x}^c)$ along x_2 axis among polygonal cross-section with $3, 4, 6, 50$ and 100 edges. Despite the singular stresses around the vertices, the interior thermoelastic stresses exhibit a flattening trend with the increase of distance h. Since the dominant function of interfacial effects on stress is $1/r$, the interfacial effects reduce rapidly. Shown as Figs. 9(c, d) and 9(e, f), the interior stresses are in similar shape though their values are different due to different temperatures. Regarding the exterior stress, all polygonal cases exhibit similar trends, which can be interpreted that the influence of ETG and eigenstrain on stress behave as $1/r$ and $1/r^2$, respectively. Fig. 7(e) and 7(f) compare stresses with a circular cross-section in an infinite medium, and their main difference exist in the neighborhood of two end-points. Since the thermoelastic field is obtained through the superposition of thermal and elastic fields, Fig. 8(c) exhibit a similar trend, although a reference temperature is applied.

6. Conclusions

The two-dimensional bimaterial elastic, thermoelastic Green's function is obtained through finite part integrals. Moreover, their domain integrals with uniform, linear and quadratic eigen-fields for two-dimensional bimaterial problems are presented. Using the transformation coordinates, the domain integrals are obtained through the direct method and Green's theorem through conversion to contour integrals. Numerical verification is conducted on DEIM, with FEM, analytical formulae for circular inhomogeneities with heat source and initial stresses. An exact thermoelastic solution of a circular inhomogeneity embedded within an infinite domain has been presented. The formulae are further applied for DEIM to investigate boundary effects of polygonal cross-sections embedded in a large concrete, where material properties are adjusted to simulate a semi-infinite problem. The aforementioned formulae for harmonic, bi-harmonic, and displacement potentials are provided for the community.

CRediT authorship contribution statement

Chunlin Wu: Conceptualization, Methodology, Data curation, Programming, Validation, Writing – original draft, Visualization. **Huiming Yin:** Resource, Writing – review & editing, Supervision, Funding acquisition.

Declaration of competing interest

The authors declare that they have no known competing financial interests or personal relationships that could have appeared to influence the work reported in this paper.

Data availability

We have provided the link to all data/model in Appendix B of the manuscript.

Acknowledgment

This work is sponsored by the National Science Foundation IIP, United States #1941244, CMMI#1762891 and U.S. Department of Agriculture NIFA #2021-67021-34201, whose support is gratefully acknowledged.

Appendix A. Transform domain integrals to other branches

A.1. Handle image terms of harmonic Φ and bi-harmonic Ψ potentials

Section 3 states that the domain integrals of Φ and Ψ can be handled by mirroring source parts ($\mathbf{x}'$). This appendix section aims to provide some simple derivations, and we have already implemented the domain integrals in the "POLYGON-EIM" package. For readers of interest, please refer to Appendix B for specific programming details with code, which contains both circular and polygonal integrals. In the following, we take $\overline{\Phi}$ and $\overline{\Phi}^p$ for instances. Following the same notation of our recent paper (Wu and Yin, 2021a),

$$\begin{aligned}
\overline{\Phi}_{,i} &= \sum_{f=1}^{N_F} (\lambda_f^0)_i \Phi_0^f(\bar{b}_f, \bar{l}_f^-, \bar{l}_f^+) \\
\overline{\Phi}_{p,i} &= Q_P \Big\{ \delta_{pi}\overline{\Phi} + (x_p - \overline{x_p}^c)\Phi_{,i} \\
&\quad + \sum_{f=1}^{N_F} (\lambda_f^0)_i \Big(\bar{b}_f (\lambda_f^0)_p \Phi_0^f(\bar{b}_f, \bar{l}_f^-, \bar{l}_f^+) + (\xi_f^0)_p \Phi_1^f(\bar{b}_f, \bar{l}_f^-, \bar{l}_f^+) \Big) \Big\}
\end{aligned} \tag{A.1}$$

where the parameters $\bar{b}_f = ((-v_f^{\pm})_i - x_i)(\lambda_f^0)_i$ and $\bar{l}_f^{\pm} = ((-v_f^{\pm})_i - x_i)(\xi_f^0)_i$. As shown in Eq. (A.1), the image terms can be well handled

by mirroring the source points. Notice that the 2DTC is based on the counterclockwise sequence. Therefore, attention should be paid to the inverse sequence of vertices of each edge.

A.2. Handle Boussinesq's displacement potentials with other branches

Section 3.2 states that the domain integrals of the other three branches can be extended from the first branch. Let us take Θ^u, Θ^u_p, Θ^u_{pq} and $\overline{\Theta}^u$, $\overline{\Theta}^u_p$, $\overline{\Theta}^u_{pq}$ as instance to illustrate the transformation process. In Eq. (8), one can obtain relationship that $\overline{\alpha}^u(\mathbf{x},\mathbf{x}') = \alpha^u(\overline{\mathbf{x}},\mathbf{x}')$. In such a case, $\overline{\Theta}^u$ can be expressed as,

$$\overline{\Theta}^u = \sum_{f=1}^{N_F} \mathcal{T}(\tilde{b}_f, \tilde{l}^+_f) - \mathcal{T}(\tilde{b}_f, \tilde{l}^-_f) \tag{A.2}$$

where the parameters $\tilde{b}_f = ((v^+_f)_i - Q_I x_i)(\lambda^0_f)_i$ and $\tilde{l}^\pm_f = ((v^\pm_f)_i - Q_I x_i)(\xi^0_f)_i$. And the partial derivatives of $\bar{\Theta}^u$ can be modified from Eq. (17) as,

$$\overline{\Theta}^u_{,i} = Q_I \sum_{f=1}^{N_F} -(\lambda^0_f)_i \Big\{ \mathcal{M}(\tilde{b}_f, \tilde{l}^+_f) - \mathcal{M}(\tilde{b}_f, \tilde{l}^-_f) \Big\} \tag{A.3}$$

Subsequently, for the second order partial derivative,

$$\begin{aligned}\overline{\Theta}^u_{,ij} = Q_I Q_J \sum_{f=1}^{N_F} -(\lambda^0_f) \Big\{ -(\lambda^0_f)_j \Big(\frac{\partial \mathcal{M}}{\partial b}(\tilde{b}_f, \tilde{l}^+) - \frac{\partial \mathcal{M}}{\partial b}(\tilde{b}_f, \tilde{l}^-)\Big) \\ - (\xi^0_f)\Big(\frac{\partial \mathcal{M}}{\partial l}(\tilde{b}_f, \tilde{l}^+) - \frac{\partial \mathcal{M}}{\partial l}(\tilde{b}_f, \tilde{l}^-)\Big) \Big\}\end{aligned} \tag{A.4}$$

where Q_J handles negative sign with respect to the second axis that $\frac{\partial \tilde{b}_f}{\partial \overline{x}_j} = -Q_J(\lambda^0_f)_j$ and $\frac{\partial \tilde{l}^\pm_f}{\partial \overline{x}_j} = -Q_J(\xi^0_f)_j$. For the other two branches, Θ^l and $\overline{\Theta}^l$, it is observed that $\alpha^l(\mathbf{x},\mathbf{x}') = -\alpha^u(\mathbf{x},\mathbf{x}')$ and $\overline{\alpha}^l(\mathbf{x},\mathbf{x}') = -\overline{\alpha}^u(\mathbf{x},\mathbf{x}')$. Hence, they can be obtained similarly to Eq. (A.1) with a negative sign. Regarding the linear domain integrals,

$$\begin{aligned}\overline{\Theta}^u_{p,i} &= \frac{\partial}{\partial x_i}\Big\{ \int_\Omega (x'_p - \overline{x}_p)\alpha^u(\overline{\mathbf{x}},\mathbf{x}')\, d\mathbf{x}' + (\overline{x}_p - x^c_p)\overline{\Theta}^u \Big\} \\ &= Q_P \overline{\Theta}^u + (\overline{x}_p - x^c_p)\overline{\Theta}^u_{,i} \\ &\quad + Q_I \sum_{f=1}^{N_F} -(\lambda^0_f)_i \Big\{ (\lambda^0_f)_p \tilde{b}_f \big(\mathcal{M}(\tilde{b}_f, \tilde{l}^+) - \mathcal{M}(\tilde{b}_f, \tilde{l}^-)\big) \\ &\quad + (\xi^0_f)_p \big(\mathcal{M}^I(\tilde{b}_f, \tilde{l}^+) - \mathcal{M}^I(\tilde{b}_f, \tilde{l}^-)\big) \Big\}\end{aligned} \tag{A.5}$$

As for the quadratic linear domain integrals,

$$\begin{aligned}\overline{\Theta}^u_{pq,i} &= \frac{\partial}{\partial x_i}\Big\{ \int_\Omega (x'_p - \overline{x}_p)(x'_q - \overline{x}_q)\alpha^u(\overline{\mathbf{x}},\mathbf{x}')d\mathbf{x}' \\ &\quad + (\overline{x}_p - x^c_p)\overline{\Theta}^u_q + (\overline{x}_q - x^c_q)\overline{\Theta}^u_p - (\overline{x}_p - x_p)(\overline{x}_q - x_q)\overline{\Theta}^u \Big\} \\ &= (\overline{x}_p - x^c_p)\overline{\Theta}^u_{q,i} + (\overline{x}_q - x^c_q)\overline{\Theta}^u_{p,i} + Q_P\delta_{pi}\overline{\Theta}^u_q + Q_Q\delta_{qi}\overline{\Theta}^u_p \\ &\quad - \big(Q_P\delta_{pi}(\overline{x}_q - x^c_q) + Q_Q\delta_{qi}(\overline{x}_p - x^c_p)\big)\overline{\Theta}^u \\ &\quad - (\overline{x}_p - x^c_p)(\overline{x}_q - x^c_q)\overline{\Theta}^u_{,i} \\ &\quad + Q_I \sum_{I=1}^{N_F} -(\lambda^0_f)_i \Big\{ (\lambda^0_f)_p(\lambda^0_f)_q \tilde{b}^2_f \big(\mathcal{M}(\tilde{b}_f, \tilde{l}^+) - \mathcal{M}(\tilde{b}_f, \tilde{l}^-)\big) \\ &\quad + \big((\lambda^0_f)_p(\xi^0_f)_q + (\lambda^0_f)_q(\xi^0_f)_p\big) \\ &\quad \tilde{b}_f\big(\mathcal{M}^I(\tilde{b}_f, \tilde{l}^+) - \mathcal{M}^I(\tilde{b}_f, \tilde{l}^-)\big) \\ &\quad + (\xi^0_f)_p(\xi^0_f)_q \big(\mathcal{M}^{II}(\tilde{b}_f, \tilde{l}^+) - \mathcal{M}^{II}\tilde{b}_f, \tilde{l}^-) \big) \Big\}\end{aligned} \tag{A.6}$$

For domain integrals with β functions can be obtained by replacing $\mathcal{M}$ with $\mathcal{N}$ and Θ with Λ functions.

Appendix B. Introduction to "POLYGON-EIM" package

This paper aims to introduce the polygonal domain integrals of thermal, thermoelastic, and elastic Green's function and to promote its versatile applications to the engineering community. Therefore, we implemented the domain integrals and Eshelby's EIM in the "POLYGON-EIM" package, which is available at homepage of Prof.Yin research group through the : link. The code was programmed mainly using namespaces that beginners of C++ can understand.

The library (header files of functions) consists of six parts, which are (i) "UNIFORM_polygon_domain_integrals", (ii) "LINEAR_polygon_domain_integrals", (iii) "QUADRATIC_polygon_domain_integrals" for uniform, linear and quadratic harmonic and bi-harmonic potential functions of Green's functions. The remaining three parts are, (iv) "UNIFORM_bimaterial", (v) "LINEAR_bimaterial", (vi) "QUADRATIC_bimaterial", which are uniform, linear and quadratic domain integrals of Boussinesq's displacement potentials. Notice that the six header files include both analytical circular and polygonal domain integrals. Readers can easily identify them, i.e., "Theta_2_ij_analytical" stands for the second derivative of quadratic circular domain integrals $\Theta_{pq,ij}$. Considering the efforts of differentiating branches, we merged branches in functions, which does not require further modification for u and $\bar{u}$ cases (used in the paper).

Properties of the matrix, thermal conductivity (k_0, k_1), stiffness (mu_0, mu_1, $nu0, nu1$), thermal modulus $ma0, ma1$ can be modified in source file "eyemat.cpp". The source points (a polygonal shape circle) can be generated automatically with specified number of edges and the center is $(0, 0.12)$m, which can be modified in "Configure.cpp". Currently, one input file " EP_MAT.txt " is needed, and we used the example in the uploaded package to illustrate it. EP_MAT.txt

```
5     1E6      0.3      0     (Thermal conductivity, shear
                               modulus, Poisson's ratio,
                               thermal modulus)
0     0.12     0              (Position of the expansion point,
                               heat source)
QUA                          (Order of eigen fields, the option
                               can be UNI, LIN, QUA)
```

This "EP_MAT.txt" is used for Fig. 5 for elastic stress comparison.

References

Barber, J.R., 1992. Elasticity. Springer Dordrecht, Dordrecht.

Brisard, S., Dormieux, L., Sab, K., 2014. A variational form of the equivalent inclusion method for numerical homogenization. Int. J. Solids Struct. 51 (3–4), 716–728.

Chiu, Y.P., 1977. On the stress field due to initial strains in a cuboid surrounded by an infinite elastic space. J. Appl. Mech. 44 (4), 587–590.

Chiu, Y.P., 1978. On the stress field and surface deformation in a half space with a cuboidal zone in which initial strains are uniform. J. Appl. Mech. 45 (2), 302–306.

Chiu, Y.P., 1980. On the internal stresses in a half plane and a layer containing localized inelastic strains or inclusions. J. Appl. Mech. 47 (2), 313–318.

Dang, Xiangxin, Liu, Yingjie, Wang, Linjuan, Wang, Jianxiang, 2019. Solutions of the elastic fields in a half-plane region containing multiple inhomogeneities with the equivalent inclusion method and the applications to properties of composites. Acta Mech. 230 (5), 1529–1547.

Dyson, F.W., 1891. The potentials of ellipsoids of variable densities. Q. J. Pure Appl. Math..

Eshelby, John Douglas, 1957. The determination of the elastic field of an ellipsoidal inclusion, and related problems. Proc. R. Soc. Lond. Ser. A. Math. Phys. Sci. 241 (1226), 376–396.

Eshelby, John Douglas, 1959. The elastic field outside an ellipsoidal inclusion. Proc. R. Soc. Lond. Ser. A. Math. Phys. Sci. 252 (1271), 561–569.

Gao, X.-L., Ma, H.M., 2010. Strain gradient solution for Eshelby's ellipsoidal inclusion problem. Proc. R. Soc. A: Math. Phys. Eng. Sci. 466 (2120), 2425–2446.

Hershey, A.V., 1954. The elasticity of an isotropic aggregate of anisotropic cubic crystals. J. Appl. Mech. 21 (3), 236–240.

Hori, Muneo, Nemat-Nasser, Sia, 1993. Double-inclusion model and overall moduli of multi-phase composites. J. Eng. Mater. Des. 116.

Hou, Peng-Fei, Jiang, Hai-Yang, Li, Qiu-Hua, 2013a. Three-dimensional steady-state general solution for isotropic thermoelastic materials with applications I: General solutions. J. Therm. Stresses 36 (7), 727–747.

Hou, Peng-Fei, Li, Qiu-Hua, Jiang, Hai-Yang, 2013b. Three-dimensional steady-state general solution for isotropic thermoelastic materials with applications II: Green's functions for two-phase infinite body. J. Therm. Stresses 36 (8), 851–867.

Kroner, Ekkehart, 1958. Berechnung der elastischen Konstanten des Vielkristalls aus den Konstanten des Einkristalls. Z. Physik 151 (4), 504–518.

Kuvshinov, Boris N., 2008. Elastic and piezoelectric fields due to polyhedral inclusions. Int. J. Solids Struct. 45 (5), 1352–1384.
Liu, Y.J., Song, G., Yin, H.M., 2015. Boundary effect on the elastic field of a semi-infinite solid containing inhomogeneities. Proc. R. Soc. A: Math. Phys. Eng. Sci. 471 (2179), 20150174.
Mori, T., Tanaka, K., 1973. Average stress in matrix and average elastic energy of materials with misfitting inclusions. Acta Metall. 21 (5), 571–574.
Moschovidis, Z.A., Mura, T., 1975. Two-ellipsoidal inhomogeneities by the equivalent inclusion method. J. Appl. Mech. 42 (4), 847–852.
Mura, Toshio, 1987. Micromechanics of Defects in Solids. Springer Netherlands, Dordrecht.
Nowacki, Witold, 1986. Thermoelasticity, Second Ed. Pergamon Press, OXford.
Nozaki, H., Taya, M., 1997. Elastic fields in a polygon-shaped inclusion with uniform eigenstrains. J. Appl. Mech. 64 (3), 495–502.
Nozaki, H., Taya, M., 2000. Elastic fields in a polyhedral inclusion with uniform Eigenstrains and related problems. J. Appl. Mech. 68 (3), 441–452.
Rodin, Gregory J., 1996. Eshelby's inclusion problem for polygons and polyhedra. J. Mech. Phys. Solids 44 (12), 1977–1995.
Ru, C.Q., 1999. Analytic solution for Eshelby's problem of an inclusion of arbitrary shape in a plane or half-plane. J. Appl. Mech. 66 (2), 315–523.
Trotta, S., Marmo, F., Rosati, L., 2017. Evaluation of the Eshelby tensor for polygonal inclusions. Composites B 115, 170–181.
Waldvogel, Jörg, 1979. The Newtonian potential of homogeneous polyhedra. Zeitschrift Für Angew. Math. Und Physik ZAMP 30 (2), 388–398.
Walpole, L.J., 1996. An elastic singularity in joined half-spaces. Internat. J. Engrg. Sci. 34 (6), 629–638.
Walpole, L., 1997. An inclusion in one of two joined isotropic elastic half-spaces. IMA J. Appl. Math. 59 (2), 193–209.
Wang, Tengxiang, Wu, Chunlin, Zhang, Liangliang, Yin, Huiming, 2022. The Green's function-based thermal analysis of a spherical geothermal tank in a semi-infinite domain. J. Appl. Mech. 89 (7), 071008.
Wu, Chunlin, Wang, Tengxiang, Yin, Huiming, 2023a. The Green's function based thermoelastic analysis of a spherical geothermal tank in a semi-infinite domain. J. Mech. Phys. Solids 173, 105207.
Wu, Chunlin, Wei, Zhenhua, Yin, Huiming, 2021a. Virtual and physical experiments of encapsulated phase change material embedded in building envelopes. Int. J. Heat Mass Transfer 172, 121083.
Wu, Chunlin, Yin, Huiming, 2021a. Elastic solution of a Polygon-shaped inclusion with a polynomial Eigenstrain. J. Appl. Mech. 88 (6).
Wu, Chunlin, Yin, Huiming, 2021b. The inclusion-based boundary element method (iBEM) for virtual experiments of elastic composites. Eng. Anal. Bound. Elem. 124, 245–258.
Wu, Chunlin, Zhang, Liangliang, Cui, Junhe, Yin, Huiming, 2022. Three dimensional elastic analysis of a bi-material system with a single domain boundary element method. Eng. Anal. Bound. Elem..
Wu, Chunlin, Zhang, Liangliang, Yin, Huiming, 2021b. Elastic solution of a polyhedral particle with a polynomial eigenstrain and particle discretization. J. Appl. Mech. 88 (12).
Wu, Chunlin, Zhang, Liangliang, Yin, Huiming, 2023b. Stress concentration of a micro-void embedded in a bi-layered material considering the boundary effects. J. Eng. Mech. 149.
Yin, H.M., Sun, L.Z., Chen, J.S., 2006. Magneto-elastic modeling of composites containing chain-structured magnetostrictive particles. J. Mech. Phys. Solids 54 (5), 975–1003.
Yu, H.Y., Sanday, S.C., 1991. Elastic fields in joined half-spaces due to nuclei of strain. Proc. R. Soc. Lond. Ser. A: Math. Phys. Sci. 434 (1892), 503–519.
Yu, H.Y., Sanday, S.C., Rath, B.B., 1992. Thermoelastic stresses in bimaterials. Phil. Mag. A 65 (5), 1049–1064.
Zaoui, André, 2002. Continuum micromechanics: Survey. J. Eng. Mech. 128 (8), 808–816.